

Hydrocarbon-Rich Groundwater above Shale-Gas Formations: A Karoo Basin Case Study

by William K. Eymold¹, Kelley Swana², Myles T. Moore¹, Colin J. Whyte¹, Jennifer S. Harkness¹, Siep Talma³, Ricky Murray⁴, Joachim B. Moortgat¹, Jodie Miller², Avner Vengosh⁵, and Thomas H. Darrah⁶

Abstract

Horizontal drilling and hydraulic fracturing have enhanced unconventional hydrocarbon recovery but raised environmental concerns related to water quality. Because most basins targeted for shale-gas development in the USA have histories of both active and legacy petroleum extraction, confusion about the hydrogeological context of naturally occurring methane in shallow aquifers overlying shales remains. The Karoo Basin, located in South Africa, provides a near-pristine setting to evaluate these processes, without a history of conventional or unconventional energy extraction. We conducted a comprehensive pre-industrial evaluation of water quality and gas geochemistry in 22 groundwater samples across the Karoo Basin, including dissolved ions, water isotopes, hydrocarbon molecular and isotopic composition, and noble gases. Methane-rich samples were associated with high-salinity, NaCl-type groundwater and elevated levels of ethane, ⁴He, and other noble gases produced by radioactive decay. This endmember displayed less negative $\delta^{13}\text{C}-\text{CH}_4$ and evidence of mixing between thermogenic natural gases and hydrogenotrophic methane. Atmospheric noble gases in the methane-rich samples record a history of fractionation during gas-phase migration from source rocks to shallow aquifers. Conversely, methane-poor samples have a paucity of ethane and ⁴He, near saturation levels of atmospheric noble gases, and more negative $\delta^{13}\text{C}-\text{CH}_4$; methane in these samples is biogenic and produced by a mixture of hydrogenotrophic and acetoclastic sources. These geochemical observations are consistent with other basins targeted for unconventional energy extraction in the USA and contribute to a growing data base of naturally occurring methane in shallow aquifers globally, which provide a framework for evaluating environmental concerns related to unconventional energy development (e.g., stray gas).

Introduction

Although horizontal drilling and hydraulic fracturing have enhanced unconventional hydrocarbon recovery throughout the last decade, there have been significant controversies regarding the cause and environmental

implications of elevated hydrocarbon gas levels in drinking-water wells in various petroleum basins in North America (e.g., Osborn et al. 2011; Warner et al. 2012a, 2014; Jackson et al. 2013; Molofsky et al. 2013; Darrah et al. 2014, 2015b; Vengosh et al. 2014; Siegel et al. 2015; Humez et al. 2016; Nicot et al. 2017a; Harkness et al. 2017b; Darrah 2018). Several studies suggest that shale-gas drilling leads to fugitive gas contamination in a subset of drinking-water wells near drill sites (Osborn et al. 2011; Jackson et al. 2013; Brantley et al. 2014; Darrah et al. 2014; Heilweil et al. 2015; Sherwood et al. 2016), while others suggest that methane is natural and unrelated to shale-gas development (Molofsky et al. 2013; Warner et al. 2013; Baldassare et al. 2014; Siegel et al. 2015; Darrah et al. 2015b; Harkness et al. 2017b).

In order to evaluate the environmental effects of hydrocarbon extraction in petroleum basins targeted for drilling, baseline groundwater quality has been evaluated using a multiple geochemical tracer approach (e.g., Molofsky et al. 2013; Darrah et al. 2014, 2015b; McMahon et al. 2015; Nicot et al. 2017a, 2017b, 2017c). These studies have identified elevated levels of methane at concentrations up to its saturation point in shallow aquifers and revealed an association between methane and NaCl-type waters, valley bottoms, faulting, and

¹School of Earth Sciences, The Ohio State University, 275 Mendenhall Laboratory, 125 South Oval Mall, Columbus, OH 43210; eymold.1@osu.edu; moore.3222@osu.edu; whyte.25@osu.edu; harkness.42@osu.edu; moortgat.1@osu.edu

²Department of Earth Sciences, Stellenbosch University, Private Bag XI, Matieland, 7602, South Africa; kelly.swana90@gmail.com; jmiller@sun.ac.za

³Natural Resources and the Environment, CSIR Pretoria, P.O. Box 395, Pretoria, 0001, South Africa; siep.talma@gmail.com

⁴Groundwater Africa, 38 Disa Ave., Kommetjie, 7975, South Africa; ricky@groundwaterafrica.co.za

⁵Division of Earth and Ocean Sciences, Nicholas School of the Environment, Duke University, Durham, NC 27708; vengosh@duke.edu

⁶Corresponding author: School of Earth Sciences, The Ohio State University, 275 Mendenhall Laboratory, 125 South Oval Mall, Columbus, OH 43210. darrah.24@osu.edu

Article impact statement: Evaluation of Karoo Basin groundwater baseline prior to hydraulic fracturing.

Received December 2017, accepted December 2017.

© 2018, National Ground Water Association.

doi: 10.1111/gwat.12637

highly reducing aquifers (Warner et al. 2012a; Jackson et al. 2013; Darrah et al. 2015a, 2015b; Harkness et al. 2017b, 2018). In general, this natural methane displayed low levels of ethane or higher aliphatic hydrocarbons (i.e., high ratio of methane to higher order hydrocarbons designated as C_1/C_2+), intermediate to less negative values for stable isotopes of methane (e.g., $\delta^{13}C-CH_4$), and a long history of multiphase hydrocarbon migration from source rocks (e.g., Marcellus Shale, Barnett Shale) to shallow aquifers based on noble gas evidence. By comparison, groundwater samples associated with either documented or interpreted anthropogenic stray gas contamination events occur across a broad range of salt contents and water types, display highly elevated levels of ethane and higher aliphatic hydrocarbons (lower C_1/C_2+) consistent with deeper hydrocarbon sources, more positive $\delta^{13}C-CH_4$, and stripping of atmospheric noble gases (Jackson et al. 2013; Brantley et al. 2014; Darrah et al. 2014, 2015a; Sherwood et al. 2016; Wen et al. 2016).

While these and other important contributions have addressed various aspects of the controversy surrounding elevated levels of hydrocarbon gases in shallow aquifers, the ongoing debate on the benefits and consequences of shale-gas development is stymied further until the groundwater community reaches a consensus on the hydrogeological context of naturally occurring methane in shallow aquifers overlying shales targeted for drilling. To this point, although it has been nearly seven years since the initial Osborn et al. (2011) paper, there is still a dearth of published genuinely predrill, baseline datasets. Although the baseline studies that have been published are of great value, the majority of these studies did not start until after unconventional shale-gas drilling had commenced in these areas (Molofsky et al. 2013; Baldassare et al. 2014; Siegel et al. 2015; Darrah et al. 2015b; Humez et al. 2016; Nicot et al. 2017a; Harkness et al. 2017b; Nicot et al. 2017b, 2017c). Thus, it remains uncertain if observations from those datasets actually represent the natural background. To further complicate the issue, most sedimentary basins targeted for unconventional development in the USA and Canada were already exposed to an extensive history of coal mining as well as legacy oil and gas exploitation, leaving an uncertain, or at least unconstrained, potential for contamination related to those anthropogenic activities. Each of these factors has led to considerable confusion about the hydrogeological context of genuinely baseline conditions for naturally occurring methane and saline waters in shallow aquifers overlying shales targeted for unconventional hydrocarbon development.

Recent work has attempted to address this issue by conducting directly paired, longitudinal studies of water quality both before and after unconventional drilling in the northern Appalachian Basin (e.g., Harkness et al. 2017b). Here, we employ a different study design strategy by examining water quality and the hydrogeological context for the occurrence of hydrocarbon gases and salts in a nearly pristine setting with neither a local history of mining nor conventional or unconventional energy

extraction in the Karoo Basin, South Africa. We designed this study to improve the groundwater community's knowledge regarding not only the presence of dissolved natural gases but also to gain a better understanding of the source and migration mechanisms of subsurface natural gas-rich fluids by examining their occurrence and geochemistry in a region unaffected by coal mining, conventional petroleum extraction, or unconventional shale-gas development. While it is unclear if these genuinely baseline data are globally representative, they comprise an important piece of evidence with which to compare existing and future datasets.

Geological and Study Background

The planned exploitation of unconventional hydrocarbon resources within the semiarid, water-restricted Karoo Basin in South Africa has necessitated a comprehensive evaluation of predrill baseline water quality data throughout the region (Murray 2015; Swana 2016). In such an environment, the consequences of compromised drinking-water quality can have significant environmental, agricultural, and human health implications. While scientists have researched the shallow groundwater networks throughout the Karoo Basin over the past five decades, major uncertainties remain about the hydrogeological context of naturally occurring methane- and salt-rich groundwater throughout the region (Murray 2015; Swana 2016).

In this study, groundwater is evaluated using a comprehensive suite of tracers, including water parameters (pH, Eh, electrical conductivity, temperature), dissolved ion chemistry (e.g., Na, Ca, Cl, Br), water isotopes (δ^2H-H_2O , $\delta^{18}O-H_2O$), major gas geochemistry (e.g., N_2), hydrocarbon gas geochemistry (C_1-C_5), compound-specific stable isotopes of hydrocarbons (δ^2H-CH_4 , $\delta^{13}C-CH_4$, $\delta^{13}C-C_2H_6$), noble gas elemental (He, Ne, Ar) and isotope geochemistry ($^3He/^4He$, $^{20}Ne/^{22}Ne$, $^{21}Ne/^{22}Ne$, $^{20}Ne/^{36}Ar$, $^{40}Ar/^{36}Ar$), and tritium (3H) following standard methods reported previously (Darrah et al. 2015b; Moore et al. 2018; Harkness et al. 2017b).

These data were collected from two subsets of samples: (1) methane-rich springs or (2) groundwater boreholes sampled near bubbling springs from across the Karoo Basin. This suite of geochemical tracers allows us to provide the first comprehensive baseline report of the groundwater characteristics for this hydrocarbon-rich region which will be followed up in a longitudinal study during and after industrial activity, develop a data base of genuinely predrill data, and expand the growing geochemical data base of methane-rich groundwaters globally.

Brief Geologic/Hydrologic Overview of the Karoo Basin

The Karoo Basin, located in South Africa, spans an area of more than 200,000 km² and underlies a majority of the country (Aarnes et al. 2011; Figure 1). This sedimentary basin developed as a large retro-arc foreland basin behind the Cape Fold Belt between the late-Paleozoic to mid-Mesozoic (Catuneanu et al. 2005). The Karoo

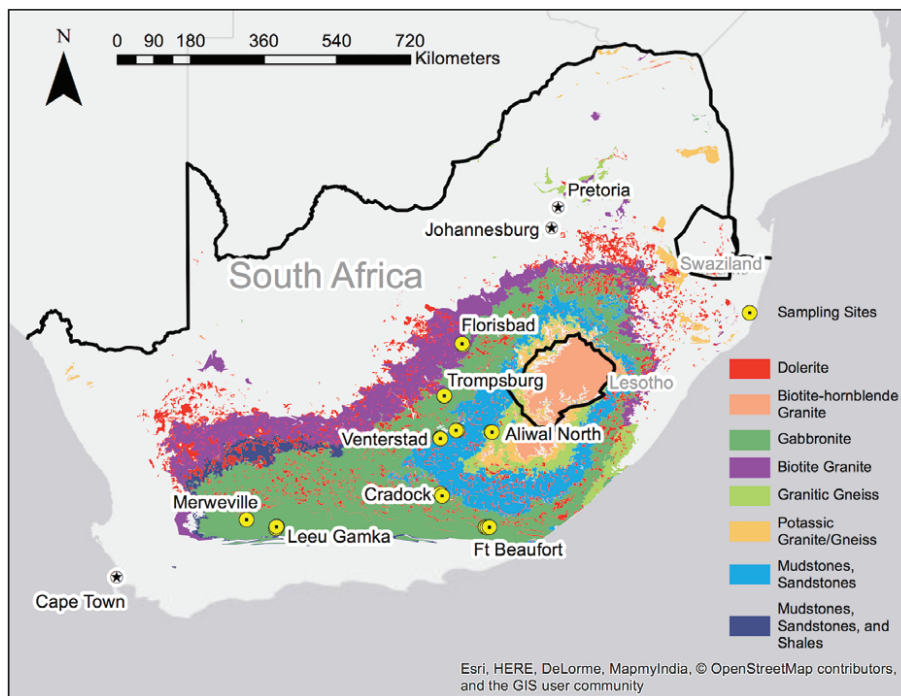


Figure 1. Map of Karoo Basin. Sampling site locations ($n = 22$) are shown as yellow circles and are associated with named sampling regions ($n = 8$). General geologic descriptions for surface lithology are indicated via color and in the legend. Note the presence of dolerite sills, dikes, and intrusions (red) throughout.

Supergroup, which includes the primary and secondary target formations for unconventional hydrocarbon development (i.e., Whitehill and Prince Albert formations), contains Carboniferous-age marine glacial deposits at its base and is comprised dominantly of interbedded terrestrial sandstones, silty carbonates, and shales deposited from the Carboniferous to mid-Jurassic (Johnson et al. 1996; Johnson et al. 2006) (Figure 2). The Permian-age Whitehill Fm., which is dominantly shale with up to 14% total organic carbon (TOC) and contains abundant carbonates and pyrite, has a thickness of 10 to 80 m and lies between the underlying Prince Albert Fm. and the superior Collingham Fm. (Johnson et al. 1996, 2006). Together with the Ripon Fm., this group of Permian-age rocks is collectively called the Eccca Group (Johnson et al. 1996, 2006; Catuneanu et al. 2005).

Most active groundwater wells in this region are producing groundwater from shallow aquifers, usually less than 200 m from the surface, while the depth to the water table varies both locally and seasonally with a typical range between 5 and 15 m from ground surface (Rosewarne et al. 2013). While preferential regional-scale groundwater flow is topographically controlled, the dominant direction varies across the Karoo Basin (Adams et al. 2001; Rosewarne et al. 2013). In the western Karoo, regional flow direction in shallow aquifers is mainly to the north, while in the central Karoo, regional flow direction in shallow aquifers is dominantly from the north down to the southwest, south, and southeast. The eastern Karoo is the most complex section, having variable flow directions in shallow aquifers in areas of the eastern sections of the Karoo (Adams

et al. 2001; Rosewarne et al. 2013). By comparison, heterogeneous, localized groundwater recharge occurs primarily during seasonal flooding events (Le Maltre et al. 2009). Most of this localized recharge occurs within fractured top-of-rock aquifers and fractured areas near dolerite dike intrusions, which dominate actively produced groundwater flow systems in the area (Mahed 2016). The actively produced aquifers include Permian-age sandstones (e.g., Waterford Fm.) and mudstones, primarily from the Eccca Group (e.g., Collingham and Fort Brown formations) and Beaufort Group (e.g., Koonap, Middleton, and Balfour formations), as well as along fractured contacts with Jurassic dolerite dykes (Adams et al. 2001). Faulting, specifically in the northern and northwest portions of the basin, provides additional pathways for heterogeneous groundwater recharge and groundwater migration (Oesterlen 1991; Johnson et al. 1996; Johnson et al. 2006). Areas of intense faulting, or fracturing near faults or dolerite intrusions, may be preferential pathways for natural gas migration, as well as zones of intense local meteoric water recharge. The groundwater residence times, flow conditions, and geochemistry of deeper wells (more than 1000 m) are relatively poorly understood (Woodford and Chevallier 2002) but recent work suggests that extensive episodes of freshwater recharge during wetter climatic conditions reduced the salinity of basinal brines (Harkness et al. 2018).

Design of the Study

The Water Resource Commission (WRC) of South Africa proposed a study to develop the baseline geochemical measurements of groundwater quality within the Karoo

Karoo Basin		Age
	Drakensberg basalts	Jurassic
Stormberg Group (Sandstone/Mudstone)	Clarens Formation	Jurassic
	Elliot Formation	Triassic- Jurassic
	Molteno Formation	Triassic
	Stratigraphic Hiatus	Triassic
Beaufort Group (Sandstone/Shale)	Burgersdorp Formation	Triassic
	Katberg Formation	
	Balfour Formation	Permian
	Koonap & Middleton	
Ecca Group (Sandstone/Shale)	Waterford and Fort Brown Formations	Permian
	Ripon Formation	
	Collingham & Whitehill	
	Prince Albert Formation	Carboniferous- Permian
	Dwyka Group	Carboniferous
	Pre-Karoo Basement	Carboniferous and older

Figure 2. Stratigraphic column for the Karoo Basin. Lithologic symbols are used to describe each formation name; formation age is provided in the right column. Target formation for shale-gas development is the Whitehill Formation (shown with the Collingham Fm.) in the Ecca Group. This formation of shales and sandstones (with TOC ~ 14%) varies in thickness between 10 and 80 m and underlies the basin between 2 and 4 km depth.

Basin prior to shale-gas exploration (Murray 2015). They sought to characterize both deep and shallow sources of groundwater by collecting samples from known bubbling methane-rich springs and nearby groundwater boreholes and then evaluating them for major ions, metals, stable isotopes of water and gas, and gas geochemistry (Murray 2015).

Our study targeted eight ($n=8$) sampling regions across the Karoo Basin that were evaluated for gas and water geochemistry (Figure 1). The sampling regions were selected based on prior knowledge of the presence of geothermal springs/artesian boreholes or the presence of deep boreholes. The study also included other nearby drinking-water or agricultural wells for comparison for a total of $n=22$ samples. Samples included two deep boreholes (at depths of ~1400 and ~4200 m), nine springs/artesian wells, and 11 groundwater samples from shallow boreholes (Murray 2015; Swana 2016). Sampling

occurred over a 2-week period between June and July 2014.

Geochemical Techniques Implemented

A comprehensive evaluation of groundwater aqueous and gas geochemistry is necessary to establish baseline geochemical measurements prior to shale-gas extraction. Data generated as part of this study are used to evaluate the content and context of methane- and salt-rich groundwaters throughout the region, and better understand the source and mechanism of hydrocarbon transport to and within shallow aquifers. This study area was chosen to expand our knowledge of the hydrogeological and geochemical context for hydrocarbon gases in an area that serves as an example of a genuinely predrill, baseline setting, thus improving our understanding of naturally occurring methane in shallow aquifers globally. Additionally, this work will help provide a framework for evaluating

environmental concerns related to unconventional energy development (e.g., stray gas). Various aspects of water stable isotopes, sources of salinity, and other aspects of water quality were presented previously (Murray 2015; Swana 2016) and elsewhere in this volume (Harkness et al. 2018). Thus, we provide only a summary on the water quality parameters in the Results and Discussion sections. The current study will focus on placing gas geochemical data, including hydrocarbon molecular and isotopic composition, and noble gas geochemistry, within the context of the hydrological setting.

The molecular composition of hydrocarbons (e.g., C_1/C_2+) and stable isotopes for hydrogen (H) and carbon (C) in methane (δ^2H-CH_4 ; $\delta^{13}C-CH_4$) and ethane ($\delta^{13}C-C_2H_6$) present in groundwater can be used to determine the genetic source (i.e., biogenic vs. thermogenic) of natural gases (Bernard et al. 1976; Schoell 1983; Whiticar et al. 1986). Thermogenic natural gases are produced by the thermocatalytic degradation of organic matter. The generation of thermogenic natural gas produces ethane and heavier aliphatic hydrocarbons (i.e., termed “wetter”) in addition to methane. Thermogenic gases display less negative stable isotope values of δ^2H-CH_4 and $\delta^{13}C-CH_4$ (e.g., $\delta^{13}C-CH_4 > -55\text{‰}$) (Bernard et al. 1976; Whiticar et al. 1986; Whiticar 1999). By comparison, biogenic natural gas is produced by methanogens and consists almost exclusively of methane and CO_2 (more than 99.9%). Biogenic CH_4 displays more negative values for $\delta^{13}C-CH_4$ between -75‰ and -55‰ (Schoell 1983). The various pathways of microbial methanogenesis impart characteristic but sometimes overlapping ranges of $\delta^{13}C-CH_4$ and δ^2H-CH_4 for both hydrogenotrophic and acetoclastic methanogenesis (Whiticar 1999). Hydrogenotrophic methanogenesis produces CH_4 with a larger fractionation from the source of organic matter (i.e., more negative $\delta^{13}C-CH_4$) than acetoclastic methanogenesis (Whiticar 1999), whereas acetoclastic methanogenesis strongly fractionates δ^2H-CH_4 . Thus, the δ^2H-CH_4 serves as an important tracer for distinguishing between natural gas produced by hydrogenotrophic and acetoclastic methanogenesis.

Following the formation of biogenic and thermogenic hydrocarbon gases, additional postgenetic processes can alter the original composition of natural gases. These processes include: (1) mixing with either other biogenic or thermogenic natural gases; (2) secondary biodegradation that consumes wet gas components, while yielding CH_4 via methanogenesis; (3) anaerobic oxidation (e.g., sulfate reduction); (4) aerobic oxidation; (5) diffusive fractionation; and (6) fractionation by solubility partitioning during fluid migration (e.g., Etiope et al. 2009; Etiope and Cicciolelli 2009; Darrah et al. 2015b). Each of these processes can alter the original composition and obfuscate the genetic source of natural gas. Alternatively, these changes provide important insights on the history of natural gas in the subsurface.

In addition to hydrocarbon composition, the inert nature and well-constrained elemental and isotopic compositions of noble gases found in the atmosphere, crust,

and mantle allow them to serve as reliable geochemical tracers of fluid mean residence time, hydrocarbon source, and transport mechanisms in groundwater (Ballentine et al. 2002). The ratios and isotopes of noble gases are distinct enough to not only discern naturally sourced fluids from those contaminated by drilling, but also to identify the specific migration mechanisms that resulted in the observed signature (Darrah et al. 2014). This consortium of analyses provides a robust set of baseline data, serves as a guideline for comparison to potentially contaminated water in future studies, and allows us to evaluate the influence and genetic source of hydrocarbon-rich fluids formed within or that migrated into shallow aquifers throughout the Karoo Basin.

Methods

Sample Collection and Field Measurements

Water samples were collected after 30 min of flushing or when the field the parameters stabilized, prior to any treatment systems, and were filtered and preserved in airtight, high density polyethylene (HDPE) bottles following USGS protocols (USGS 2011). Samples were filtered through $0.45\ \mu\text{m}$ filters for dissolved ions. Water chemistry samples were stored on ice or refrigerated until the time of their analysis.

At each of these locations, field measurements were conducted including temperature, pH, oxidation-reduction potential, alkalinity, and electroconductivity (EC) using a YSI multiprobe calibrated daily. Hydrocarbon gas samples were collected in closed volume, refrigeration-grade copper tubes that were flushed in-line with at least 50 volumes of sample water prior to sealing with stainless steel clamps following methods reported previously (Darrah et al. 2015b; Kang et al. 2016). Noble gas samples were collected in duplicate copper tubes following the same methods established above. Both sample splits were shipped to the Ohio State University (OSU) for sample analysis.

Analytical Methods

Methods and data related to major dissolved ions, water stable isotopes, and trace element isotopes (e.g., B, Sr) were analyzed by standard methods (Warner et al. 2012a, 2014) and presented elsewhere in this volume (Harkness et al. 2018). Dissolved gas samples were measured by extracting the fluid from the copper sampling tubes on a vacuum line following standard methods (Darrah et al. 2013; Kang et al. 2016; Harkness et al. 2017a). From this gas volume, splits of samples were taken for the measurement of major gas components (e.g., N_2 , O_2 , CO_2 , CH_4 to C_5H_{12}), noble gases (e.g., He), and stable carbon and hydrogen isotopes (e.g., $\delta^{13}C-CH_4$).

The major and hydrocarbon gases for each sample were measured using an Scientific Research Instruments gas chromatograph (GC) at OSU following methods reported previously (Darrah et al. 2015b; Kang et al.

Table 1
Field Parameters and Water Chemistry for Groundwater Samples from the Karoo Basin.

Town	Date	Location	Sample No.	Temp °C	pH	EC µS/cm	TDS mg/L	ORP mV	DO mg/L	Alk mg/L	Cl mg/L	δ ² H-H ₂ O per mille (‰)	δ ¹⁸ O-H ₂ O per mille (‰)	DIC (mg/L)	δ ¹³ C DIC per mille (‰)
Florisbad	06/28/14	Florisbad Spa	FLS1	20.0	9.4	3620	2160	49	3.3	2	1300	-37.7	-5.8	22	-32.3
	06/28/14	Farm	FLB5	19.2	7.7	1382	822	72	4.1	240	136	-21.5	-3.6	444	-4.7
Trompsbur	06/29/14	Valkfontein	VFB1	29.5	9.2	10,190	6100	184	1.9	14	4100	-39.1	-6.5	25	-19.1
	06/29/14	Valkfontein	VFB2	18.2	7.7	502	301	43	4.5	130	12.0	-29.0	-3.7	284	-9.4
	06/29/14	Vlakfontein	VFB4	19.3	7.5	712	525	49	4.6	—	25.6	-28.1	-4.4	324	-9.4
	06/30/14	Aliwal North	ANS1	30.0	9.1	2010	1200	197	2.5	24	665	-36.7	-6.0	20	-11.6
Venterstad	06/30/14	Farm	ANBH1	21.6	7.5	1896	1123	45	2.2	25	546	-37.0	-5.6	73	-19.8
	07/01/14	Rooiwal	RWB1c	25.7	8.0	487	293	-205	1.8	170	26.9	-30.9	-4.9	227	-4.7
	07/01/14	Rooiwal	RWB5	18.1	7.4	854	511	29	4.0	280	20.2	-28.3	-4.4	465	-12.3
	07/02/14	Vaalbank	VBB1	18.2	8.4	543	322	-157	1.9	94	77.3	-32.5	-4.7	167	-9.0
	07/02/14	La Rochelle	LRB1	17.4	7.1	1231	735	45	4.0	350	48.3	-21.1	-3.3	585	-11.5
Fort	07/02/14	La Rochelle	LRB2	17.3	7.5	580	345	49	4.5	216	10.1	-27.3	-4.2	339	-9.6
	07/04/14	Sulphur Baths	BFB1	23.5	10.0	822	492	-232	1.5	30	174	-41.6	-6.0	63	16.4
	07/04/14	Sulphur Baths	BFB2	21.2	7.4	2000	1194	-220	1.5	244	436	-25.5	-4.3	403	-13.3
	07/04/14	Rocky Ridge	RRB1	21.2	7.1	2490	1480	35	3.9	418	524	-25.7	-4.0	622	-11.2
	07/06/14	Cradoek Spa	CRS1	29.4	9.8	208	123	-210	1.6	28	20.9	-41.5	-6.7	55	-3.1
Leeu	07/06/14	Waalkraal farm	DRB4	16.2	7.8	1615	963	41	4.0	612	42.3	-12.3	-1.7	764	-15.4
	07/08/14	Kruidfontein	WP508	26.5	8.1	930	557	-172	4.4	140	76.2	-29.9	-4.3	212	-15.1
	07/08/14	Groot	WP502	20.3	7.9	527	316	24	5.7	172	24.1	-4.3	0.7	236	-11.1
	07/08/14	Groot	WP505	23.5	8.2	1326	799	-190	1.5	178	91.7	-29.8	-4.2	232	-17.6
Merweville	07/09/14	Farm	SAL/66	—	—	—	—	—	—	—	3600	—	—	—	—
	07/09/14	Farm	MWB2	21.5	7.1	1067	639	27	3.4	252	103	-30.6	-4.8	347	-13.5
			MIN	16.2	7.1	208	123	-232	1.5	2	10	-41.6	-6.7	20	-32.3
			MAX	30.0	10.0	10,190	6100	197	5.7	612	4100	-4.3	0.7	764	16.4
			MEAN	21.8	8.1	1666	1000	-24	3.2	181	548	-28.7	-4.4	281	-11.3
		STD	4.2	0.9	2117	1265	135	1.3	156	1114	10.4	1.7	211	8.9	

Samples Which Were Not Analyzed Are Denoted by a Hyphen.

Table 2
Hydrocarbon Molecular and Isotopic Signatures for Groundwater Samples from the Karoo Basin.

Town	Date	Location	Sample No.	CH ₄ ccSTP/kg	C ₂ H ₆ ccSTP/kg	C ₃ H ₈ ccSTP/kg	C ₁ /C ₂ +	$\delta^2\text{H-CH}_4$ per mille (‰)	$\delta^{13}\text{C-CH}_4$ per mille (‰)	$\delta^{13}\text{C-C}_2\text{H}_6$ per mille (‰)
Florisbad	06/28/14	Florisbad Spa	FLS1	32.0	1.32×10^{-2}	4.70×10^{-4}	2334	-197.5	-50.90	-36.26
	06/28/14	Farm	FLB5	3.40	1.14×10^{-3}	5.70×10^{-5}	2845	-201.1	-51.60	-36.31
Trompsbur	06/29/14	Vlaktefontein	VFB1	1.00	b.d.l.	—	5915	-188.0	-65.65	-35.94
	06/29/14	Vlaktefontein	VFB2	1.21	b.d.l.	—	9869	-282.7	-72.14	-39.84
	06/29/14	Vlaktefontein	VFB4	2.02	b.d.l.	—	32,414	b.d.l.	—	—
Aliwal	06/30/14	Aliwal North	ANS1	35.3	7.72×10^{-3}	5.40×10^{-4}	4271	-204.0	-64.98	-37.61
	06/30/14	Farm	ANBH1	39.1	7.59×10^{-3}	b.d.l.	4877	-196.0	-65.61	-36.75
Venterstad	07/01/14	Rooiwal	RWB1c	2.91	7.95×10^{-4}	—	3655	-199.9	-50.68	—
	07/01/14	Rooiwal	RWB5	0.01	—	—	36,683	b.d.l.	—	—
	07/02/14	Vaalbank	VBB1	5.31	1.85×10^{-3}	5.37×10^{-4}	2228	-206.4	-49.54	-35.87
	07/02/14	La Rochelle	LRB1	2.24	b.d.l.	—	51,470	-278.6	-71.49	—
Fort	07/02/14	La Rochelle	LRB2	1.61	b.d.l.	—	16,547	-269.5	-73.14	-42.15
	07/04/14	Sulphur Baths	BFB1	0.01	—	—	—	b.d.l.	—	—
	07/04/14	Sulphur Baths	BFB2	23.5	4.56×10^{-3}	9.74×10^{-4}	4255	-207.7	-55.36	-35.29
	07/14/14	Rocky Ridge	RRB1	3.67	7.53×10^{-4}	—	4879	-211.7	-55.88	-36.15
Cradock	07/06/14	Cradock Spa	CRS1	0.22	b.d.l.	—	15,247	-248.4	-72.11	-41.06
	07/06/14	Waaikraal farm	DRB4	3.07	1.89×10^{-4}	—	16,247	-258.0	-70.14	-40.84
Leeu	07/08/14	Kruidfontein	WP508	0.07	b.d.l.	—	7989	b.d.l.	—	—
	07/08/14	Groot	WP502	1.14	b.d.l.	—	12,484	-263.1	-74.45	-42.65
	07/08/14	Groot	WP505	0.27	b.d.l.	—	9451	-209.2	-67.64	—
Merweville	07/09/14	Farm	SA1/66	—	—	—	—	—	—	—
	07/09/14	Farm	MWB2	1.05	b.d.l.	—	14,120	-270.5	-74.61	—
			MIN	0.01	7.53×10^{-4}	5.70×10^{-5}	2228	-282.7	-74.61	-42.65
			MAX	39.1	1.32×10^{-2}	9.74×10^{-4}	51,470	-188.0	-49.54	-35.29
			MEAN	7.57	4.70×10^{-3}	5.00×10^{-4}	12,889	-229.0	-63.88	-38.21
		STD	12.7	4.49×10^{-3}	2.93×10^{-4}	13,078	34.2	9.36	2.68	

Samples With Concentrations Below Detection Limits Are Signified by "b.d.l.," Whereas Samples That Were Not Analyzed Are Denoted by a Hyphen.

2016). The average external precision was determined by measurement of a "known-unknown" standard, including an atmospheric air standard (Lake Erie, Ohio Air) and a series of synthetic natural gas standards obtained from Praxair. The results of the "known-unknown" average external precision analysis are as follows: CH₄ (1.27%), C₂H₆ (1.68%), C₃H₈ (1.34%), N₂ (1.25%), and CO₂ (1.06%). CH₄ concentrations are reported as ccSTP/kg of water (the SI molar unit for gas abundance in water) at standard temperature and pressure (STP), where 1 mg/kg of gas is equivalent to 1.4 ccSTP/kg.

Procedures for analyses of stable isotopic values of carbon in methane and ethane were described previously (Jackson et al. 2013; Darrah et al. 2015b). Chromatographic separation of gas compounds was performed using a Thermo Fisher Trace Ultra GC and the isotopic values were measured using a dual-inlet Thermo Fisher Delta V Plus isotope ratio mass spectrometer (Thermo Fisher Scientific, Waltham, Massachusetts). With this combination, the detection limits for $\delta^{13}\text{C-CH}_4$, $\delta^2\text{H-CH}_4$, and $\delta^{13}\text{C-C}_2\text{H}_6$ were 0.001, 0.005, and 0.001 ccSTP/kg, respectively. The $\delta^{13}\text{C-CH}_4$ and $\delta^{13}\text{C-C}_2\text{H}_6$ values are expressed in per mille (designated hereafter as ‰) versus the international standard Vienna Pee Dee belemnite (VDPD), with a standard deviation of $\pm 0.1\%$, while $\delta^2\text{H-CH}_4$ are expressed in per mille vs. the international

standard Vienna Standard Mean Ocean Water (VSMOW) with a standard deviation of $\pm 0.5\%$.

The abundance and isotopic composition of noble gases were determined using a Thermo Fisher Helix SFT Noble Gas MS at OSU following methods reported previously (Darrah and Poreda 2012; Darrah et al. 2013). The average external precisions based on "known-unknown" standards were all less than $\pm 1.46\%$ for noble gas concentrations with values reported in parentheses (⁴He (0.78%), ²²Ne (1.46%), and ⁴⁰Ar (0.38%)). These values were determined by measuring referenced and cross-validated laboratory standards, including an established atmospheric standard (Lake Erie Air) and a series of synthetic natural gas standards obtained from Praxair, including known and validated concentrations of CH₄ to C₅H₁₂ hydrocarbons, N₂, CO₂, H₂, O₂, and each of the noble gases. Noble gas isotopic standard errors were approximately ± 0.0091 times the ratio of air (or 1.26×10^{-8}) for the ³He/⁴He ratio, less than $\pm 0.402\%$ and $\pm 0.689\%$ for ²⁰Ne/²²Ne and ²¹Ne/²²Ne, respectively, and less than ± 0.643 and $\pm 0.427\%$ for ³⁸Ar/³⁶Ar and ⁴⁰Ar/³⁶Ar, respectively (higher than typical because of interferences from C₃H₈ on mass = 36 and 38).

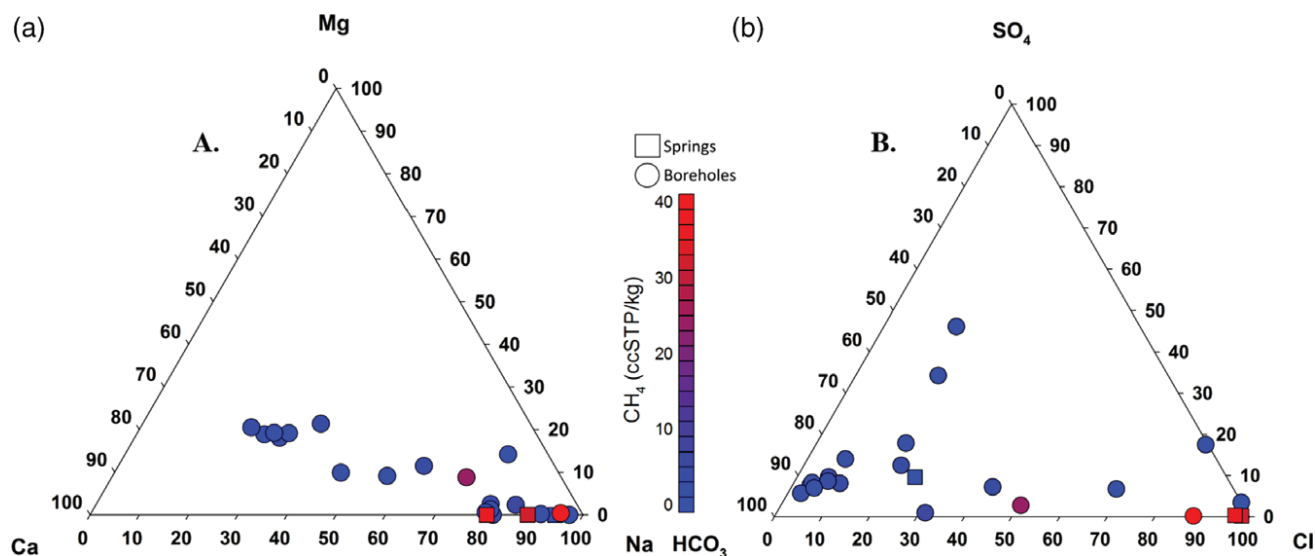


Figure 3. Ternary diagrams of the major cations, Ca vs. Mg vs. Na (A) and major anions, HCO₃ vs. SO₄ vs. Cl (B) in Karoo Basin groundwater. The majority of samples appear to fall along a mixing line between two groundwater types: (1) a fresh groundwater type with a Ca-Mg-HCO₃ composition and (2) a saline water type with a NaCl composition. Samples with [CH₄] exceeding 14 ccSTP/kg (the U.S. Department of Interior limit for methane in groundwater) were observed exclusively in NaCl-type groundwaters.

Presentation of Data

All maps, cross sections, and well coordinates are plotted using ArcMap GIS 10.3 (ESRI, Redlands, California). Additional published hydrocarbon data from the Karoo region were taken from (Talma and Esterhuysen 2015). All graphics are plotted using Sigma Plot 12.3. Statistical evaluations including mean, minima, maxima, standard deviation, and Pearson correlations were performed using SPSS v. 24 (IBM, Armonk, New York). The correlation coefficient r^2 reported in the text was calculated as Pearson's correlation coefficient, and corresponding p -values are provided throughout the text.

We present data from this study with color-coded symbols based on the abundance of methane, where low methane concentrations close to 0 ccSTP/kg are blue and range up to red for methane concentrations of 40 ccSTP/kg (i.e., the level of methane saturation in groundwater at 10 °C). Data from previous studies are identified by empty green shapes which reflect the source of the data (namely, circles for boreholes, squares for springs, and triangles for coalbed gases).

Results

Dissolved Ion Chemistry

Field parameters and water chemistry data are presented in Table 1. Groundwater pH values varied between 7.1 and 10.0. Groundwater temperatures ranged from 16.2 to 30.0 °C. Redox state ranged from oxidizing to highly reducing conditions, with field oxidation-reduction potentials (ORP) from -232 to +197 mV. Salinity of the groundwater varied over three orders of magnitude, while electrical conductivity ranged from 208 to 10,190 μS/cm and total dissolved solids (TDS) ranged from 123 to 6100 mg/kg.

Dissolved ion and water stable isotope data are reported elsewhere in this volume (Harkness et al. 2018). Briefly, the Cl content of the samples ranged from relatively freshwater (10.1 mg/L) to saline water (4100 mg/L) (Table 2), while Br concentrations ranged from 0.1 to 23.4 mg/L, and DIC (as bicarbonate) from 20 to 764 mg/L (Harkness et al. 2018). Overall, samples from this study area are dominantly comprised of three endmembers: (Type A) low salinity Ca-HCO₃ water, (Type B) low salinity Na-HCO₃-Cl water, and (Type C) a relatively high salinity, NaCl water endmember (Swana 2016; Harkness et al. 2018) (Figure 3).

Hydrocarbon and Major Gases

Hydrocarbon data are presented in Table 2. CH₄ concentrations varied from near method detection limits (0.01 ccSTP/kg) to near the saturation limits of methane in water (39.1 ccSTP/kg). Ethane (C₂H₆) ranged from below method detection limits (0.0005 ccSTP/kg) to 0.0132 ccSTP/kg. Propane (C₃H₈) was above detection limits (5×10^{-5} ccSTP/kg) in seven samples in which the concentrations ranged between 5.70×10^{-5} and 9.74×10^{-4} ccSTP/kg. The corresponding ratios of C₁/C₂+ ranged from 2228 to 51,470 (Table 2; Figure 4).

CH₄ was strongly correlated to C₂H₆ ($r^2 = 0.930$, $p < 0.01$) and all methane-rich waters (defined here as methane concentrations exceeding 14 ccSTP/kg based on the U.S. Department of Interior action level) displayed propane above the method detection limits. While there was a statistically significant positive correlation between CH₄ and Cl ($r^2 = 0.81$, $p < 0.01$) that correlation is driven by a strong correlation between these parameters in the top quartile of methane concentrations (i.e., there is significantly greater scatter in samples with lower

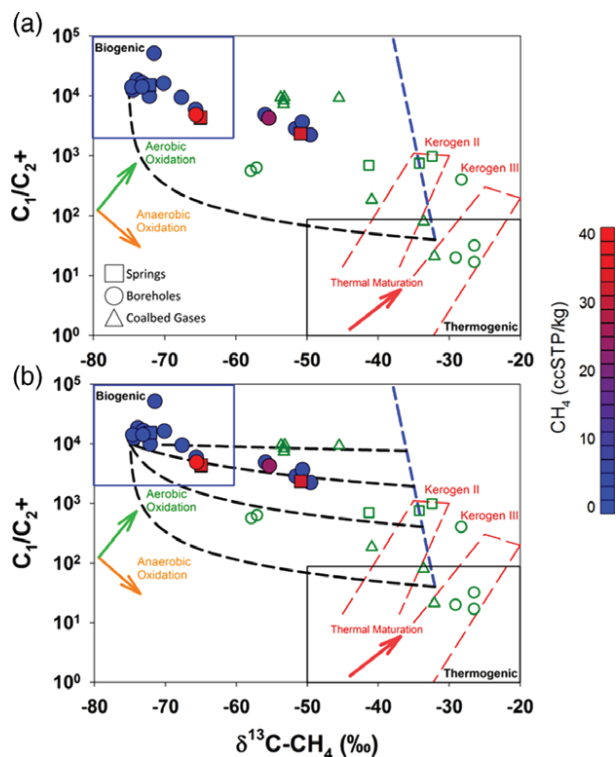


Figure 4. Ratio of methane to higher-order aliphatic hydrocarbons (C_1/C_{2+}) vs. stable isotopic composition of carbon in methane ($\delta^{13}C-CH_4$) of gases dissolved in groundwaters collected in this study and those from previously published groundwater studies in the Karoo Basin (Talma and Esterhuysen 2015; denoted by green outlined symbols used here and in subsequent figures). The typical ranges for thermogenic and biogenic methane compositions are shown as black and blue boxes, respectively (Bernard et al. 1976). The green and orange arrows show postgenetic, microbial alteration by aerobic and anaerobic oxidation, respectively. The blue trend line displays postgenetic alteration from the theoretical thermogenic endmember following fractionation by solubility partitioning of the hydrocarbon gas components assuming a GGS-R fractionation model (adapted from Darrah et al. 2015 and Harkness et al. 2017a). The black mixing lines depict hypothetical mixing between (1) a theoretical thermogenic endmember that was progressively modified by solubility partitioning during fluid migration and (2) a biogenic gas. The majority of samples appear to fall along a mixing trend between biogenic sources and a migrated thermogenic gas that previously altered by solubility partitioning. All high methane samples appear to fall on a mixing line between fluids that have undergone two-phase advection (most likely from a deeper thermogenic source) that later mix with a biogenic endmember.

methane concentrations, including one anomalous sample [VFB1] that has an exceptionally high Cl concentration [4100 mg/kg], but little methane [1.0 ccSTP/kg] (Tables 1 and 2; Figure 3).

Hydrocarbon stable isotope data are presented in Table 2 and Figures 4–6. The carbon isotopic signature for CH_4 ($\delta^{13}C-CH_4$) ranged from -74.61‰ to -49.54‰ , while the hydrogen isotope values for CH_4 (δ^2H-CH_4) ranged from -282.7‰ to -188.0‰ (Figures 4 and 5). The $\delta^{13}C-CH_4$ values correlated negatively with C_1/C_{2+} ($r^2 = -0.566$, $p < 0.01$; Figure 4). The

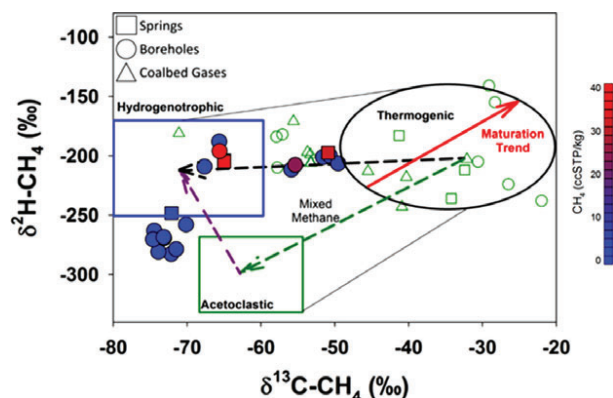


Figure 5. Stable isotopic values of hydrogen (δ^2H-CH_4) vs. carbon ($\delta^{13}C-CH_4$) in methane from samples collected in this study and those from previously published groundwater studies in the Karoo Basin (Talma and Esterhuysen 2015). The black oval represents the typical range of thermogenic natural gases, with the red arrow indicating the trend of increasing thermal maturity (Schoell 1983; Whiticar et al. 1986). The blue and green boxes represent methane produced by hydrogenotrophic methanogenesis and acetoclastic methanogenesis, respectively (Schoell 1983; Whiticar et al. 1986). The dashed black arrow represents two-component mixing between methane produced from thermogenic and hydrogenotrophic methanogenesis, while the dashed green arrow represents two-component mixing between methane produced from thermogenic and acetoclastic methanogenesis. The purple dashed arrow represents mixing between natural gases produced by acetoclastic methanogenesis and hydrogenotrophic methanogenesis. The majority of methane-rich samples appear to fall along a mixing line between thermogenic natural gas and hydrogenotrophic microbial methane, while low-methane samples plot as an ambiguous mixture of methane produced by biogenic sources.

carbon isotope values for C_2H_6 ($\delta^{13}C-C_2H_6$) ranged from -42.65‰ to -35.29‰ and correlated negatively with $\delta^{13}C-CH_4$ ($r^2 = -0.566$, $p < 0.01$) and C_1/C_{2+} ($r^2 = -0.895$, $p < 0.01$) (Figure 6).

Nitrogen (N_2) and noble gas data are presented in Table 3. Dissolved N_2 concentrations ranged between 11.03 and 24.76 ccSTP/kg (average of 14.42 ccSTP/kg, excluding the anomalously high value of 24.76 ccSTP/kg in sample VFB1; Figure 7). Except for this anomalous sample (VFB1), which also yielded a highly non-atmospheric $^{40}Ar/^{36}Ar$ of 967.16, these N_2 values are within approximately 30% of the anticipated air-saturated water (ASW) values assuming recharge at 1200 m, $15^\circ C$, and a salinity of 10 mg/kg chloride (Figure 7; Table 3). The ^{36}Ar (a noble gas isotope incorporated into groundwater exclusively from atmospheric sources) concentrations for the majority of samples ranged from 828 to 1562×10^{-6} ccSTP/kg (average [^{36}Ar] of 1184×10^{-6} ccSTP/kg) (Table 3; Figure 7). The sample with an anomalously high N_2 concentration displayed partially stripped values of atmospheric ^{36}Ar ($[^{36}Ar] = 561 \times 10^{-6}$ ccSTP/kg). Excluding this sample, the ^{36}Ar values are within approximately 35% of the anticipated ASW values assuming recharge at 1200 m, $15^\circ C$, and a salinity of 10 mg/kg Cl. The

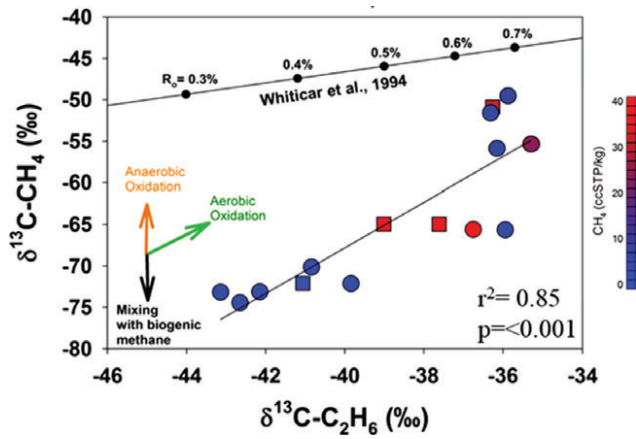


Figure 6. The carbon isotopes of methane ($\delta^{13}\text{C-CH}_4$) vs. ethane ($\delta^{13}\text{C-C}_2\text{H}_6$) from samples collected in this study. The black dotted trend line shows the anticipated change in gas isotopic composition as a source rock undergoes thermal maturation, with vitrinite reflectance values indicative of maturity. The orange arrow displays the anticipated trends for aerobic oxidation inorganically or by microbes. The green arrow displays the anticipated trends for anaerobic oxidation by methanotrophs. The black arrow displays mixing that occurs following the addition of biogenic methane. The data suggest that dissolved gases in the current study area consist of natural gas produced across a range of thermal maturities that later mixed with varying proportions of microbial methane.

^{20}Ne (also incorporated into groundwater exclusively from atmospheric sources) ranges from 131 to 527×10^{-6} ccSTP/kg (average of 272×10^{-6} ccSTP/kg), excluding the anomalously high N_2 sample that is partially stripped and contained only 121×10^{-6} ccSTP/kg (Table 3; Figure 7). The upper range of ^{20}Ne concentrations is nearly three times the anticipated values for ASW recharged in this region. Neon concentrations correlate positively with CH_4 ($r^2 = 0.780$, $p < 0.01$) and C_2H_6 ($r^2 = 0.817$, $p < 0.01$) concentrations and negatively to C_1/C_2+ ($r^2 = -0.500$, $p = 0.015$).

Helium concentrations ranged from $[\text{He}] = 48.2 \times 10^{-6}$ ccSTP/kg, which is near the ASW value of 40.5×10^{-6} ccSTP/kg to 0.483 ccSTP/kg ($[\text{He}] = 483,493 \times 10^{-6}$ ccSTP/kg) or $11,938$ times the anticipated ASW values of helium (Table 3). These values corresponded to He/Ne ratios from 0.190 , which is near ASW value of 0.230 to 3011 (Figure 8). Helium concentrations were highly correlated to methane ($r^2 = 0.623$, $p < 0.01$), ethane ($r^2 = 0.740$, $p < 0.01$), Cl ($r^2 = 0.798$, $p < 0.01$), and Br ($r^2 = 0.7$, $p < 0.001$) (Figure 9). Except for sample VFB1 from Trompsberg, groundwater samples with the highest concentrations of ^4He also displayed the highest CH_4 concentrations (Figure 9).

Helium isotopic values (i.e., $^3\text{He}/^4\text{He}$), presented as R/R_A , where R is the ratio of ^3He to ^4He in a sample compared to the ratio of ^3He to ^4He in air ($R_A = 1.384 \times 10^{-6}$), ranged between $0.0114 R_A$ and $1.1562 R_A$ (Table 3; Figure 8). The upper limit of this range suggests that the helium content is dominated by contributions from ASW and small

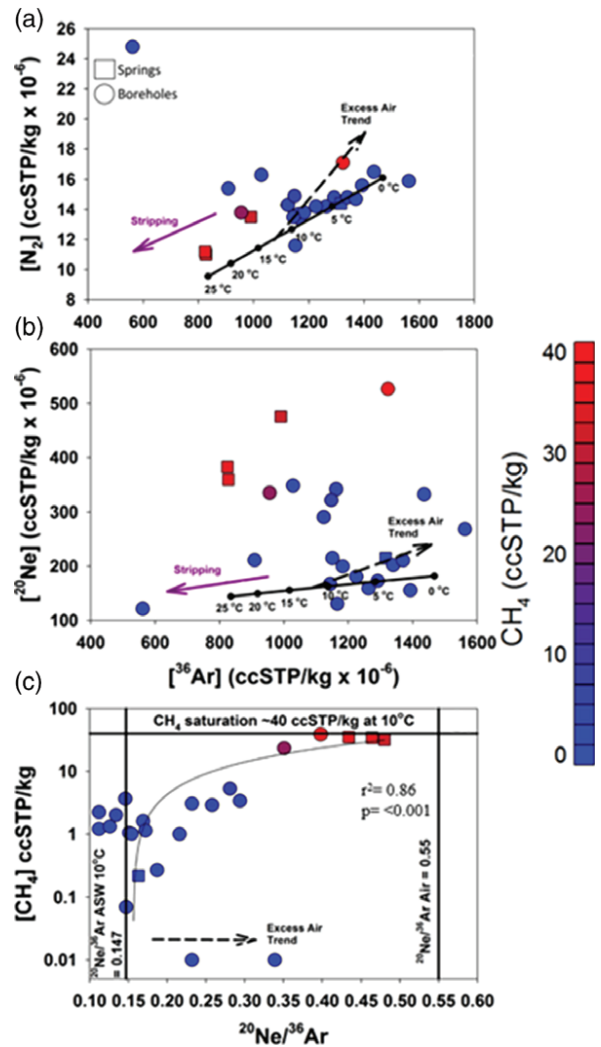


Figure 7. The concentrations of N_2 (A) and ^{20}Ne (B) vs. ^{36}Ar and the concentration of methane vs. the ratio of $^{20}\text{Ne}/^{36}\text{Ar}$ (C) from samples collected in this study. The majority of samples display N_2 and ^{36}Ar within 30% and 35% of their anticipated ASW levels, respectively, based on local groundwater recharge conditions with the exception of one anomalous sample which displays nearly twice the anticipated ASW levels of N_2 and partial stripping of ^{36}Ar and ^{20}Ne . The subset of methane-rich samples also displays elevated levels of exogenous ^{20}Ne .

contributions of ^3He ingrowth following the decay of tritium (Harkness et al. 2018). There is a trend of decreasing $^3\text{He}/^4\text{He}$ values with both increasing concentrations of ^4He and increasing ratios of He/Ne . Although four samples (VFB4, BFB1, LRB1, and RWB5) contain quantifiable mantle contributions ($\sim 1\%$) and elevated methane concentrations, the correlation of increasing $^4\text{He}/^{20}\text{Ne}$ with decreasing $^3\text{He}/^4\text{He}$ indicates that the majority of helium is predominantly from a crustal/radiogenic source (Figure 8). The $^3\text{He}/^4\text{He}$ ratio also displays significant negative correlations to $\delta^{13}\text{C-CH}_4$ ($r^2 = -0.686$; $p < 0.01$), $\delta^{13}\text{C-C}_2\text{H}_6$ ($r^2 = -0.797$; $p < 0.01$), and C_1/C_2+ ($r^2 = 0.797$; $p < 0.01$).

Neon and argon isotope ratios provide additional information about the source, water-rock interactions, and

Table 3
Noble Gas Concentrations, Noble Gas Isotopic Ratios, and Tritium for Groundwater Samples from the Karoo Basin.

Town	Date	Location	Sample No.	N ₂ ccSTP/kg	⁴ He ×10 ⁻⁶ ccSTP/kg	²⁰ Ne ×10 ⁻⁶ ccSTP/kg	³⁶ Ar ×10 ⁻⁶ ccSTP/kg	³ He/ ⁴ He R/R _A	⁴ He/CH ₄ ×10 ⁻⁶	²⁰ Ne/ ²² Ne	²¹ Ne/ ²² Ne	²⁰ Ne/ ³⁶ Ar	³⁸ Ar/ ³⁶ Ar	⁴⁰ Ar/ ³⁶ Ar	Tritium (T.U.)	CH ₄ / ³⁶ Ar
Florisbad	06/28/14	Florisbad Spa	FLS1	13.54	483.493	476	991	0.0267	15.131	9.684	0.0354	0.480	0.1930	439.65	1.6	3.2259
	06/28/14	Farm	FLB5	13.71	7568	342	1162	0.1153	2225	9.760	0.0291	0.294	0.1860	299.67	1.3	2926
Trompsburg	06/29/14	Vlakfontein	VFB1	24.76	406.302	121	561	0.0516	406.302	9.412	0.0472	0.216	0.1921	967.16	0.1	—
	06/29/14	Vlakfontein	VFB2	15.58	186	155	1393	0.4408	153	9.762	0.0289	0.112	0.1904	296.52	1.0	869
Aliwal North	06/29/14	Vlakfontein	VFB4	14.79	48.2	173	1291	1.1562	24	9.894	0.0289	0.134	0.1894	295.68	3.1	1566
	06/30/14	Aliwal North	ANS1	11.03	235.141	359	828	0.0877	6664	9.657	0.0432	0.434	0.1910	346.65	0.5	42,636
Venterstad	06/30/14	Farm	ANBHI	17.11	120.583	527	1323	0.0967	3087	9.475	0.0345	0.398	0.1880	308.64	0.1	29,519
	07/01/14	Rooiwal	RWB1c	14.27	39.636	291	1124	0.0184	13.644	9.716	0.0315	0.258	0.1898	319.54	0.5	2585
	07/01/14	Rooiwal	RWB5	15.38	87.1	211	909	0.7134	6525	9.781	0.0294	0.232	0.1844	299.48	1.2	14.7
	07/02/14	Vaalbank	VBB1	14.88	6753	322	1147	0.0420	1272	9.698	0.0311	0.281	0.1829	321.45	0.6	4627
	07/02/14	La Rochelle	LRB1	13.37	62.3	131	1166	0.7520	28	9.800	0.0276	0.112	0.1880	294.88	0.5	1924
	07/02/14	La Rochelle	LRB2	13.79	980	200	1183	0.1590	609	9.764	0.0301	0.169	0.1880	296.48	1.2	1362
Fort Beaufort	07/04/14	Sulphur Baths	BFB1	16.34	71.2	348	1028	1.0163	5025	9.789	0.0284	0.339	0.1884	296.18	0.0	13.8
	07/04/14	Sulphur Baths	BFB2	13.79	84.513	335	956	0.0236	3592	9.711	0.0321	0.351	0.1899	325.37	0.4	24,618
Cradock	07/04/14	Rocky Ridge	RRB1	13.49	10.153	167	1144	0.0118	2765	9.901	0.0320	0.146	0.1865	304.65	0.5	3211
	07/06/14	Cradock Spa	CRS1	14.39	412	215	1316	0.2654	1834	9.821	0.0295	0.163	0.1867	295.15	0.5	171
Leeu Gamka	07/06/14	Waatkraal farm	DRB4	16.46	987	333	1436	0.2113	321	10.019	0.0304	0.232	0.1854	295.25	3.1	2140
	07/08/14	Kruidfontein	WP508	14.24	14,146	181	1225	0.0114	194,466	9.891	0.0291	0.147	0.1915	317.70	0.1	59.4
	07/08/14	Groot	WP502	15.93	639	268	1562	0.3441	561	9.723	0.0290	0.172	0.1898	298.44	3.5	728
	07/08/14	Groot	WP505	11.64	62,532	215	1151	0.0183	229,185	10.027	0.0331	0.187	0.1923	304.59	0.4	237
	07/09/14	Farm	SA166	—	—	—	—	—	—	—	—	—	—	—	—	—
	07/09/14	Farm	MWB2	14.75	189	202	1339	0.6570	180	9.815	0.0276	0.151	0.1879	296.54	1.4	785
	07/09/14	Farm	MIN	11.03	48.2	121	561	0.0114	24	9.412	0.0276	0.112	0.1829	294.88	0.0	13.8
			MAX	24.76	483.493	527	1562	1.1562	4.6302	10.027	0.0472	0.480	0.1930	967.16	3.5	42,636
			MEAN	14.92	70,213	265	1154	0.2961	42,552	9.767	0.0318	0.238	0.1886	343.79	1.0	7613
			STD	2.69	137,510	110	226	0.3552	104,395	0.147	0.0050	0.109	0.0027	146.38	1.0	13,055

Samples That Were Not Analyzed Are Denoted by a Hyphen.

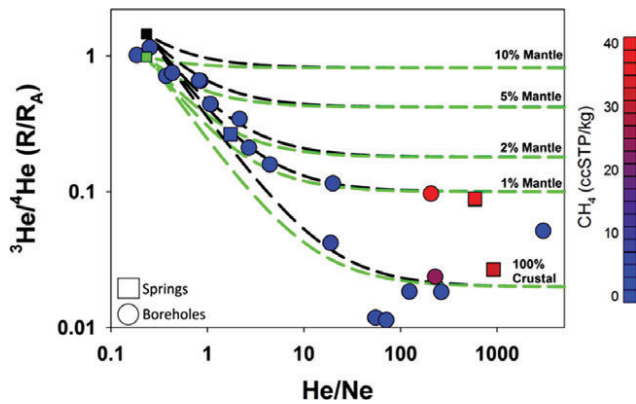


Figure 8. A comparison of the helium isotopic ratio $^3\text{He}/^4\text{He}$ (shown as R/R_A , where R_A is the ratio of $^3\text{He}/^4\text{He}$ in atmospheric air; $R_A = 1.384 \times 10^{-6}$) vs. the ratio of He/Ne of gases dissolved from groundwater collected in the Karoo Basin. The green and black boxes denote the globally constrained values for ASW (green) and tritiated ASW (black) endmembers, respectively. The dashed lines represent mixing between these endmembers and crustal helium across a range of mantle contributions. The majority of samples fall along two-component mixing lines between meteoric water (with varying degrees of tritiogenic ^3He contributions) and crustal helium. Nonetheless, we note a resolvable mantle contribution in a subset of samples with elevated methane and helium concentrations.

residence time of groundwater (Figures 10 and 11). The $^{20}\text{Ne}/^{22}\text{Ne}$ and $^{21}\text{Ne}/^{22}\text{Ne}$ ratios ranged from 9.412 to 10.027 and from 0.0276 to 0.0472, respectively (Table 3; Figure 11). The $^{40}\text{Ar}/^{36}\text{Ar}$ and $^{38}\text{Ar}/^{36}\text{Ar}$ ratios ranged from 294.88 (where ASW is 295.5) to 967.16 and from 0.1829 to 0.1930, respectively (Table 3; Figure 11). Both the neon and argon isotope values range from near ASW levels (i.e., $^{21}\text{Ne}/^{22}\text{Ne} = 0.0289$ and $^{40}\text{Ar}/^{36}\text{Ar} = 295.5$) to quantifiable excesses of noble gases produced from radioactive decay, where the abundance of ^{21}Ne and ^{40}Ar produced by radioactive decay are denoted by $^{21}\text{Ne}^*$ and $^{40}\text{Ar}^*$, respectively (Hunt et al. 2012). The $^{21}\text{Ne}/^{22}\text{Ne}$ correlates significantly to the proportion of ^4He ($r^2 = 0.818$, $p < 0.001$), salinity (Cl: $r^2 = 0.831$, $p < 0.001$; Br: $r^2 = 0.767$, $p < 0.001$), the concentrations of methane and other hydrocarbon gases (e.g., CH_4 : $r^2 = 0.582$, $p = 0.003$; C_2H_6 : $r^2 = 0.510$, $p = 0.015$), and hydrocarbon stable isotopes of hydrogen ($\delta^2\text{H}-\text{CH}_4$: $r^2 = 0.666$, $p = 0.001$) (Tables 2 and 3; Figure 11). The $^{40}\text{Ar}/^{36}\text{Ar}$ also correlates strongly to ^4He ($r^2 = 0.695$, $p < 0.001$) and salinity (Cl: $r^2 = 0.98$, $p < 0.001$; Br: $r^2 = 0.99$, $p < 0.001$). While we do observe a general trend of increasingly radiogenic $^{40}\text{Ar}/^{36}\text{Ar}$ ratios with increasing concentrations of CH_4 (Figure 9) and hydrocarbon stable isotopes of carbon (Figure 11), these trends are not statistically significant.

There are other gas isotope ratios that provide important clues about the ratios of gas and water, gas and groundwater transport mechanisms, and gas-water and water-rock interactions that occur in the subsurface (Darrah et al. 2014, 2015b; Moore et al. 2018; Figure 12). The $\text{CH}_4/^{36}\text{Ar}$ serves as a proxy for

the relative abundance of natural gas and ASW irrespective of any gas-water partitioning that may have occurred. The $\text{CH}_4/^{36}\text{Ar}$ (gas/water ratio) in this study ranges from 13.8 to 42,636 and correlates to C_2H_6 ($r^2 = 0.913$, $p < 0.01$), Cl ($r^2 = 0.819$, $p < 0.01$), and ^4He ($r^2 = 0.833$, $p < 0.01$). The $^4\text{He}/\text{CH}_4$ ratio is a sensitive indicator of biogenic vs. thermogenic contributions and water-gas interactions. The $^4\text{He}/\text{CH}_4$ ratios ranged from 24 to 406,302 and correlate significantly to Cl ($r^2 = 0.724$, $p < 0.01$) and Br ($r^2 = 0.775$, $p < 0.01$). The fractionation of the $^{20}\text{Ne}/^{36}\text{Ar}$ ratios record diagnostic partitioning between the gas and water phases during fluid transport. The $^{20}\text{Ne}/^{36}\text{Ar}$ ratios ranged from 0.112 to 0.480 and correlated to CH_4 ($r^2 = 0.852$, $p < 0.01$), C_2H_6 ($r^2 = 0.912$, $p < 0.01$), $\delta^{13}\text{C}-\text{CH}_4$ ($r^2 = 0.547$, $p = 0.012$), $\delta^{13}\text{C}-\text{C}_2\text{H}_6$ ($r^2 = 0.517$, $p = 0.048$), C_1/C_2+ ($r^2 = -0.509$, $p = 0.013$).

Discussion

The nearly pristine nature of the Karoo Basin, South Africa, provides a rare opportunity to determine the hydrogeological context for the presence of naturally occurring hydrocarbon gases in a setting with neither a local history of mining nor conventional or unconventional energy extraction. In this volume, Harkness et al. (2018) demonstrate that groundwater in this region represents a mixture between multiple sources of shallow freshwater (i.e., defined therein as Type A: $\text{Ca}-\text{HCO}_3$ and Type B: $\text{Na}-\text{HCO}_3-\text{Cl}$) and various ranges of contributions from an exogenous source of high-salinity, NaCl waters (defined therein as Type C). Similarly, we observe broad ranges in levels of hydrocarbon gases and levels of exogenous noble gases produced by radioactive decay. The levels of each of these parameters provide important clues that inform us about (1) the occurrence of naturally occurring hydrocarbon gases in a genuinely predrill, baseline study; (2) the genetic sources of hydrocarbon gases; (3) the relative contributions (i.e., mixtures) of deep, hydrocarbon-rich saline fluids in shallow aquifers; and (4) the pathways and mechanism(s) for the migration of these fluids to shallow aquifers.

The Presence of Naturally Occurring Hydrocarbon Gases in a Pristine Shallow Aquifer

All samples contained measurable and quantifiable concentrations of methane. Methane concentrations from the current study ranged up to 39.1 ccSTP/kg. Importantly, this value approaches, but does not exceed, the calculated saturation conditions for methane in freshwater in this region (saturation for $[\text{CH}_4]$ is ~ 40 ccSTP/kg at $P(\text{CH}_4) = 1$ atm with normal levels of air-saturated water gases [predominantly N_2] at 10°C at 1200 m elevation). These data support previous observations of methane concentrations at or below saturation conditions in baseline samples thought to be unaffected by shale-gas

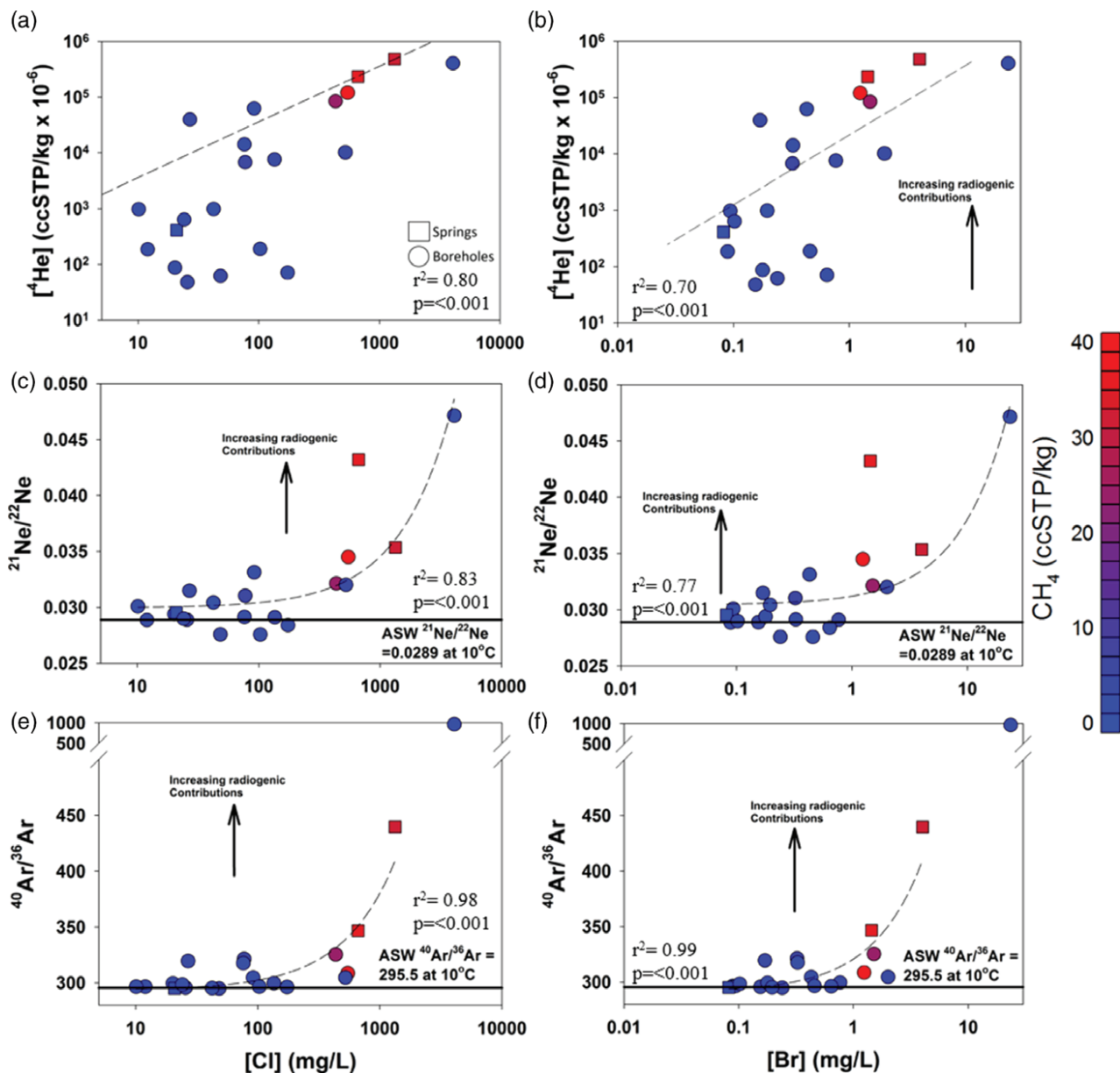


Figure 9. The concentration of [Cl] vs. ^4He (A); $^{21}\text{Ne}/^{22}\text{Ne}$ (B); and $^{40}\text{Ar}/^{36}\text{Ar}$ (C) and [Br] vs. ^4He (D); $^{21}\text{Ne}/^{22}\text{Ne}$ (E); and $^{40}\text{Ar}/^{36}\text{Ar}$ (F) from samples collected in this study. Linear regressions (dashed lines), r^2 , and p -values of the regression for all data are shown in each plot. The majority of samples display a significant correlation between noble gases produced by radioactive decay (^4He , $^{21}\text{Ne}^*$, and $^{40}\text{Ar}^*$) and brine components (i.e., Cl, Br) indicating mixing between a regional brine and relatively fresh meteoric water.

drilling in other areas. Furthermore, this upper range of concentrations reinforces the premise that conditions of gas saturation (i.e., bubble point) in regional groundwater both regulate the concentration of methane and physically control the migration of naturally occurring methane within shallow aquifers.

Typical of all petroleum basins, the complex tectonic history of the Karoo Basin has led to a diverse suite of hydrocarbon sources and the occurrence of preferential fluid migration pathways. As a result, there is a correspondingly diverse nature of groundwater geochemical compositions and groundwater quality in the shallow aquifers from this region. Similar to observations in other basins around the world, elevated methane concentrations

(defined here as greater than 14 ccSTP/kg or 10 mg/L) corresponded to samples that also displayed elevated levels of salts with a NaCl composition (defined as Type C in Harkness et al. 2018), ethane, and ^4He concentrations. In other basins, the relationship between methane, ethane, chloride, and ^4He has been attributed to the migration of a hydrocarbon-rich brine from source rocks to shallow aquifers over unknown periods of geological time (Warner et al. 2012a; Warner et al. 2012b; Jackson et al. 2013). These data reinforce our hypothesis for a common origin and migration process for an exogenous hydrocarbon-rich brine that apparently migrated to and mixed with fresh groundwater within shallow aquifers across the study area.

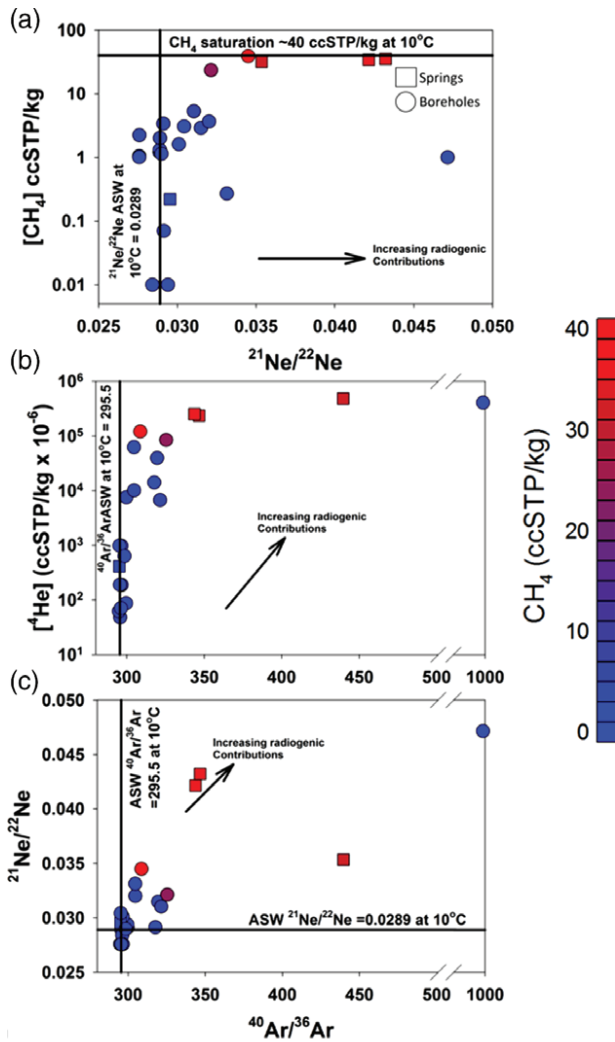


Figure 10. A comparison of methane concentration $[CH_4]$ vs. the ratio of $^{21}Ne/^{22}Ne$ (A); the concentration of helium $[^4He]$ vs. the argon isotopic composition $^{40}Ar/^{36}Ar$ (B); and the ratio of $^{21}Ne/^{22}Ne$ vs. the argon isotopic composition $^{40}Ar/^{36}Ar$ from samples collected in this study. The solid black lines depict anticipated ASW values. We note a significant increase in radiogenic noble gases (4He , $^{21}Ne^*$, $^{40}Ar^*$) in the methane-rich endmembers, supporting the hypothesis for mixing between biogenic and thermogenic natural gas.

In comparison to the methane- and salt-rich NaCl waters, the two low-chloride, fresh water endmembers displayed significantly lower methane, helium, and ethane concentrations. One notable exception from this study is a sample collected from a deep borehole in Trompsburg (VFB1), which displayed the highest salinity and one of the highest 4He concentrations recorded in the study but only contained 1 ccSTP/kg of methane.

The Sources of Naturally Occurring Hydrocarbon Gases in Shallow Aquifers

Traditional Hydrocarbon Tracers

Hydrocarbon gas within groundwater can be produced in shallow aquifers by biogenic (via microbes) or

thermogenic processes, or result from subsurface migration from an exogenous source of biogenic or thermogenic gas (Darrah et al. 2015a, 2015b). Typically, the source or genetic origin of hydrocarbon gases in shallow aquifers is determined by a combination of the molecular composition of gases (e.g., the ratio of methane $[C_1]$ to higher-order hydrocarbons $[C_2+]$, or C_1/C_2+), the stable isotopic compositions of methane (e.g., δ^2H-CH_4 , $\delta^{13}C-CH_4$), and where possible the stable isotopic composition of heavier aliphatic hydrocarbons (e.g., $\delta^{13}C-C_2H_6$) (Jackson et al. 2013; Harkness et al. 2017b). Here, we integrate hydrocarbon molecular and isotopic compositions and noble gases to provide important constraints on the genetic sources and proportions of biogenic and thermogenic natural gas, and to validate the use of noble gases as a source tracer in shallow aquifers.

In the current study, most samples with low methane concentrations (<14 ccSTP/kg) display extremely high C_1/C_2+ and very negative $\delta^{13}C-CH_4$ ($\leq \sim 70\%$) (Figure 4). Data from these samples are consistent with contributions from a purely microbial source of natural gas in shallow aquifers (blue box in Figure 4). It should be noted that the subset of samples with a nearly pure microbial molecular and isotopic hydrocarbon composition displays low salt contents (fresh water) and are dominantly found in the low salinity water types (Types A and B from Harkness et al. 2018). Conversely, the subset of methane-rich contains higher levels of ethane (and in some cases propane), displayed C_1/C_2+ ratios between 2334 and 4877, and relatively more enriched isotopic signatures for carbon ($\delta^{13}C-CH_4 = \sim -65$ to -50%) (Figure 4). Because ethane is not produced by microbial processes, its presence in the Karoo Basin suggests that a resolvable mixture of thermogenic gases likely influences these samples. However, we note that the combination of high C_1/C_2+ and intermediate $\delta^{13}C-CH_4$ values is inconsistent with any known thermogenic sources of natural gas.

A comparison of the stable isotopes of hydrogen (δ^2H-CH_4) and carbon ($\delta^{13}C-CH_4$) in methane also distinguishes low-methane and low-salinity samples from their high methane counterparts. The subset of low methane plots between hydrogenotrophic and acetoclastic microbial endmembers, and indicates a nearly pure biogenic source of methane present in the low salinity groundwater (Figure 5). While these low-methane samples appear to cluster near the hypothetical hydrogenotrophic-acetoclastic mixing line, they display more negative $\delta^{13}C-CH_4$ than a simple two-component mixture from these two sources (Figure 5). Conversely, while the methane- and salt-rich samples display significant proportions of hydrogenotrophic (microbial) methane, most samples plot along a two-component mixing trend between hydrogenotrophic (microbial) methane and an unidentified thermogenic natural gas endmember (Figure 5). Similar observations have been reported in shallow aquifers around the USA and Canada, reinforcing the interpretation that (1) there is a mixture of thermogenic natural gas in shallow aquifers overlying the Karoo and (2)

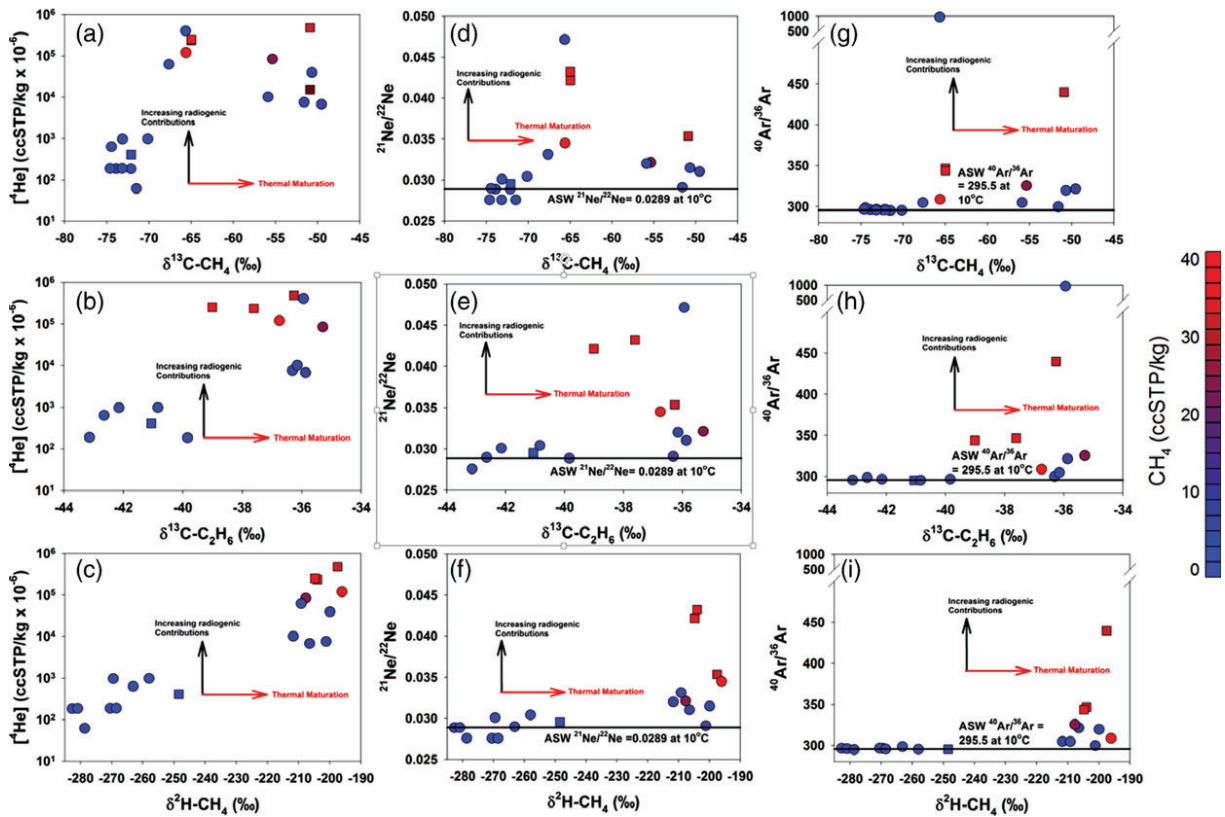


Figure 11. A comparison of $[^4\text{He}]$ (A to C); $^{21}\text{Ne}/^{22}\text{Ne}$ (D to F), and $^{40}\text{Ar}/^{36}\text{Ar}$ (G to I) vs. $\delta^{13}\text{C}-\text{CH}_4$ (A; D; G); $\delta^{13}\text{C}-\text{C}_2\text{H}_6$ (B; E; H); $\delta^2\text{H}-\text{CH}_4$ (C; F; I) from samples collected in this study. We note a general trend of corresponding increase in radiogenic noble gases and less negative values of $\delta^{13}\text{C}-\text{CH}_4$, $\delta^{13}\text{C}-\text{C}_2\text{H}_6$, and $\delta^2\text{H}-\text{CH}_4$. These data suggest that increased abundances of radiogenic noble gases correspond to more thermogenic-like stable isotopes of hydrocarbon gases.

mixing between hydrogenotrophic (microbial) methane and thermogenic natural gas occurs commonly and naturally in shallow aquifers overlying petroleum systems (Revesz et al. 2012; Jackson et al. 2013; Darrah et al. 2015b; Harkness et al. 2017b).

A comparison of $\delta^{13}\text{C}-\text{CH}_4$ and $\delta^{13}\text{C}-\text{C}_2\text{H}_6$ reinforces the interpretation that a low abundance of thermogenic natural gas is present in these samples (Figure 6). When thermogenic natural gas is generated by increasing heat and pressure, the isotopic signatures for both methane and ethane evolve simultaneously with increasing temperature along a generally linear trend and record important clues about the genetic source, thermal maturity, and subsequent postgenetic alteration of natural gases (Whiticar et al. 1994). In general, the $\delta^{13}\text{C}-\text{C}_2\text{H}_6$ values from this study area are consistent with the expected composition of thermogenic gases derived from either marine (e.g., shale) or terrestrial (e.g., coal) organic matter (Whiticar et al. 1994). The broad range of $\delta^{13}\text{C}-\text{C}_2\text{H}_6$ (-42.65‰ to -35.29‰) equates to vitrinite reflectance values of approximately $0.33\%R_0$ to $0.72\%R_0$ (solid black line in Figure 6) (Whiticar et al. 1994). These vitrinite reflectance values correspond to temperature ranges between thermally immature ($\sim 50^\circ\text{C}$) to the peak of the oil window ($\sim 80^\circ\text{C}$) and an apparent burial depth of approximately 1.75 to 3 km. The methane-rich samples typically plot on the higher end of the apparent thermal

maturity range and display $\delta^{13}\text{C}-\text{C}_2\text{H}_6$ values equivalent to a vitrinite reflectance of approximately $0.5\%R_0$ to $0.72\%R_0$, which is within the oil window (60 to 80°C).

Although the $\delta^{13}\text{C}-\text{C}_2\text{H}_6$ values provide important clues about both the presence and thermal character of thermogenic natural gas, our data are inconsistent with the simplistic evolution of a thermogenic natural gas (Figure 6). Because all of our samples fall below the anticipated thermal maturation line, we suggest that the combination of $\delta^{13}\text{C}-\text{CH}_4$ and $\delta^{13}\text{C}-\text{C}_2\text{H}_6$ data indicate significant mixtures of biogenic methane with variable contributions of natural gas derived from an unidentified thermogenic source, consistent with the other hydrocarbon data mentioned above.

The Utility of Noble Gas Tracers for Determining the Genetic Source of Natural Gas

The application of traditional molecular and isotopic hydrocarbon tracers can be complicated by uncertainties in overlapping isotopic composition of endmembers, mixing, and postgenetic modification (Whiticar 1999; Etiopie et al. 2009; Darrah et al. 2015b; Vinson et al. 2017). Because they are not altered by chemical reactions or microbial oxidation, noble gases present an advantageous addition to studies of natural gas geochemistry. Still, there are a limited number of studies that have attempted to integrate noble gases with traditional hydrocarbon molecular and

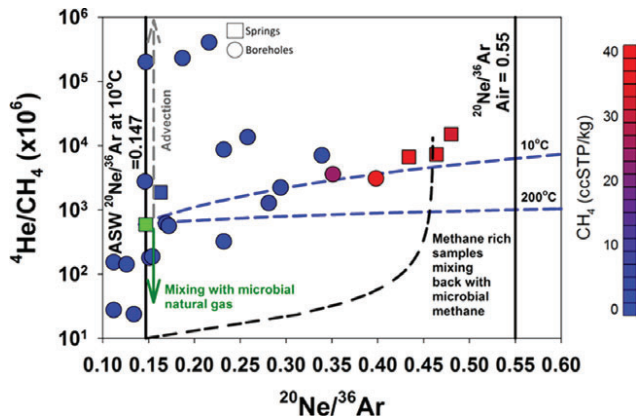


Figure 12. A plot of $^4\text{He}/\text{CH}_4$ vs. $^{20}\text{Ne}/^{36}\text{Ar}$ from samples collected in this study. The green square represents a theoretical thermogenic endmember for the Collingham Fm. based on age and U/Th concentrations. The dashed gray arrow represents one-phase advection of a thermogenic-like gas source. The solid green arrow represents mixing of thermogenic-like production gas with a “young” biogenic source. The dashed blue trend lines represent temperature-dependent two-phase advection of a thermogenic-like gas from depth to the surface. The black dashed line represents a hypothetical mixing between a migrated thermogenic source with a young biogenic source. Two-phase solubility fractionation and advection trends are based on the two-stage groundwater gas stripping and redissolution (GGS-R) model developed in Darrah et al. (2015b). Methane-rich samples appear consistent with two-phase migration of natural gas from depth to the shallow aquifers.

isotopic geochemistry in groundwater studies (Jackson et al. 2013; Darrah et al. 2014, 2015a, 2015b; Wen et al. 2016; Harkness et al. 2017b).

Similar to ethane, ^4He and heavier crustal noble gases ($^{21}\text{Ne}^*$, $^{40}\text{Ar}^*$) occur at elevated levels in older, higher temperature thermogenic natural gases, whereas recently formed microbial gases are nearly devoid of ethane or radiogenic noble gases (Darrah et al. 2015b; Harkness et al. 2017b; Hunt et al. 2012; Moore et al. 2018). Our data reveal significant correlations between various hydrocarbon tracers and the levels of the crustal noble gases ^4He , $^{21}\text{Ne}^*$, and $^{40}\text{Ar}^*$ in groundwater samples from this region. Each of the noble gases produced by radioactive decay (^4He , $^{21}\text{Ne}^*$, and $^{40}\text{Ar}^*$) included in this study correlate to each other and to various hydrocarbon tracers, suggesting a clear presence of thermogenic methane. Radiogenic ^4He correlates to both CH_4 and C_2H_6 ($r^2 = 0.623$, $p = 0.001$; $r^2 = 0.740$, $p < 0.01$), salinity (Cl [$r^2 = 0.798$, $p < 0.001$]), as well as $\delta^2\text{H}-\text{CH}_4$ ($r^2 = 0.603$, $p = 0.005$) (Figures 9 and 11). Similarly, $^{21}\text{Ne}^*$ correlates strongly with CH_4 ($r^2 = 0.909$, $p < 0.001$) and C_2H_6 ($r^2 = 0.893$, $p < 0.001$) concentrations, whereas $^{40}\text{Ar}^*$ correlates with salinity (Cl [$r^2 = 0.591$, $p = 0.005$]), and displays generally higher $\delta^{13}\text{C}-\text{CH}_4$, $\delta^2\text{H}-\text{CH}_4$, and $\delta^{13}\text{C}-\text{C}_2\text{H}_6$ values (Figures 9 and 11). Consistent with our interpretations of hydrocarbon molecular and isotopic composition, each of these observations supports the presence of thermogenic methane and validates the use of radiogenic noble

gases as a tracer for thermogenic natural gas in shallow aquifers.

Noble gases can also be a powerful suite of tracers for resolving the presence of exogenous fluids, discerning the processes that bring salt-rich natural gases to shallow aquifers, and providing a genetic fingerprint of migrated gases. As discussed in Harkness et al. (2018), the presence of extremely high ^4He concentrations up to $483,493 \times 10^{-6}$ ccSTP/kg (or approximately 1.07×10^4 times atmospheric levels) greatly exceed atmospheric contributions and/or the maximum plausible endogenous sources. Moreover, the presence of these extremely high ^4He concentrations that correlate with hydrocarbon tracers of thermogenic gases (ethane, less negative $\delta^{13}\text{C}-\text{CH}_4$ and $\delta^2\text{H}-\text{CH}_4$) and $\delta^{13}\text{C}-\text{C}_2\text{H}_6$) in groundwater samples with elevated (thermogenic) methane and salts suggests that an exogenous source of relatively old groundwater migrated into the shallow aquifers within the Karoo Basin and mixed with an apparently young, tritium-active source of meteoric waters.

While the extremely high ^4He concentrations unequivocally indicate the presence of exogenous fluids in shallow aquifers from the Karoo Basin, other major gas and noble gas isotope data provide important clues about the source and migration processes that brought exogenous fluids to the shallow aquifer. Because atmospheric gases, namely ^{20}Ne , N_2 , and ^{36}Ar , have a nearly uniform starting composition, with small differences related to changes in temperature, salinity, and elevation (atmospheric pressure), they have proven to be a useful tracer for identifying the history of hydrocarbon-rich brine migration (Darrah et al. 2014; Barry et al. 2016) and serving as a diagnostic indicator of migrated gases (Darrah et al. 2015a, 2015b; Harkness et al. 2017b; Moore et al. 2018). For example, elevated concentrations of ^{20}Ne or an increase in the $^{20}\text{Ne}/^{36}\text{Ar}$ without a corresponding increase in other atmospheric noble gases (i.e., ^{36}Ar) are diagnostic of solubility fractionation during two-phase (free gas + brine) fluid migration. Notably, we observe a marked excess in ^{20}Ne and highly elevated ratios of $^{20}\text{Ne}/^{36}\text{Ar}$ in samples with elevated salt, ^4He , and methane and ethane levels, and less negative $\delta^{13}\text{C}-\text{CH}_4$ and $\delta^2\text{H}-\text{CH}_4$ values in this study. The thermogenic methane-rich endmember displays $^{20}\text{Ne}/^{36}\text{Ar}$ ratios significantly above the ASW equilibrium value of approximately 0.147 (up to 0.480; Figure 7). Importantly, the increase in $^{20}\text{Ne}/^{36}\text{Ar}$ relates almost exclusively to an increase in ^{20}Ne concomitantly with $[\text{CH}_4]$, $[\text{C}_2\text{H}_6]$, and $[\text{He}]$ but without any observable increases (small decrease is observed) in $[\text{Ar}]$, precluding increased levels of air in these samples (Figure 7). Based on these observations, we conclude that the source of thermogenic natural gas is an exogenous fluid that has experienced multiple-stage, two-phase partitioning during fluid transport (secondary hydrocarbon migration) from its source (yet to be identified) to shallow aquifers across the region.

Similar processes of solubility partitioning that fractionated the $^{20}\text{Ne}/^{36}\text{Ar}$ ratio during fluid transport can also

account for the range of $^4\text{He}/\text{CH}_4$ in the thermogenic end-member. The relative concentration of exogenous ^4He in crustal fluids (e.g., $^4\text{He}/\text{CH}_4$, $^4\text{He}/^{20}\text{Ne}$) results from a combination of the ^4He released within the original thermogenic natural gas source and the subsequent modification that occurs during postgenetic alteration processes (e.g., fluid migration, oxidation, and methanogenic inputs) (Darrah et al. 2014, 2015a; Moore et al. 2018; Harkness et al. 2017b). While one-phase (gas dissolved in brine) migration or mixing between thermogenic and biogenic gases would be associated exclusively with enrichment of ^4He and hence $^4\text{He}/\text{CH}_4$ (Darrah et al. 2014, 2015a; Harkness et al. 2017b), the paired enrichment of $^4\text{He}/\text{CH}_4$ and $^{20}\text{Ne}/^{36}\text{Ar}$ is consistent with two-phase fluid migration (Darrah et al. 2014). These data further support our conclusion that the exogenous thermogenic natural gas migrated to the shallow aquifers, presumably along preferential pathways, as a two-phase fluid.

Resolving the Unidentified Thermogenic Endmember

While both traditional molecular and isotopic hydrocarbon and noble gas approaches individually point to the naturally occurring presence of thermogenic natural gas in shallow aquifers with a highly ambiguous composition, a parsimonious explanation requires careful integration of all data. The simultaneous presence of higher C_1/C_2+ values than any known (or at least documented) thermogenic endmembers, yet heavier $\delta^{13}\text{C}-\text{CH}_4$ values than any known (or at least documented) biogenic endmembers is confounding. Interestingly, these observations from Karoo are consistent with previous observations from other petroleum basins around the world (Darrah et al. 2014, 2015b; Moore et al. 2018; Harkness et al. 2017b).

The need to understand the source of this apparently thermogenic methane is not simply esoteric or academic as it is becoming increasingly apparent in the published literature that this poorly defined source of natural gas is common in many aquifers overlying petroleum systems and provides a useful template to understand the diagnostic geochemical signatures of natural hydrocarbon gas migration to shallow aquifers and conduct stray gas investigations (Etiope et al. 2009; Darrah et al. 2014, 2015b; Harkness et al. 2017b). Yet, despite the importance and preponderance of these trends, there is relatively little discussion about the implications of these data in the literature (Jackson et al. 2013; Darrah et al. 2014, 2015b; Moore et al. 2018; Harkness et al. 2017b) and previous studies that have identified this trend have struggled to converge on a consensus for the cause of natural gas with this composition.

Because of the presence of elevated C_1/C_2+ values, the most common interpretation for this composition is mixing between biogenic methane and thermogenic natural gas. The issue with this interpretation is that the observed composition falls along a convex mixing line (rapid increase of C_1/C_2+ followed by a decreasing

$\delta^{13}\text{C}-\text{CH}_4$) as opposed to the concave mixing line (rapid decrease of $\delta^{13}\text{C}-\text{CH}_4$ following by an increasing C_1/C_2+), the latter of which fits simple two-component mixing between biogenic and thermogenic sources (Darrah et al. 2015b; Moore et al. 2018; Harkness et al. 2017b). Previously, this convex trend has been variably attributed to a complex three-component mixing (Osborn et al. 2011; Revesz et al. 2012), diffusion (Prinzhofer and Pernaton 1997), solubility partitioning (Etiope et al. 2009; Darrah et al. 2014, 2015b; Harkness et al. 2017b), or oxidation by various potential mechanisms (Etiope et al. 2009; Etiope and Cicciooli 2009; Vinson et al. 2017).

We propose that it is useful to view the traditional hydrocarbon molecular and isotopic tracers in light of all of the geochemical data and consider the potential for postgenetic modification during fluid transport. The combination of elevated C_1/C_2+ , intermediate to heavy $\delta^{13}\text{C}-\text{CH}_4$, exogenous ^4He (and other noble gases produced by radioactive decay), and elevated $^{20}\text{N}/^{36}\text{Ar}$ in this dataset, which is consistent with a growing body of data from aquifers overlying other petroleum basins, sheds light on this poorly defined thermogenic endmember. Here, we describe an *ad hoc* interpretation based on two-phase (gas + water) solubility partitioning to explain this endmember. While this interpretation is clearly *ad hoc*, it does attempt to find a parsimonious interpretation that integrates all of the geochemical results and produce a viable explanation for both elevated C_1/C_2+ and intermediate to heavy $\delta^{13}\text{C}-\text{CH}_4$ in naturally occurring hydrocarbon gases in shallow aquifers.

During the multiple-phase fluid migration (gas + water) of thermogenic natural gas, a two-phase thermogenic natural gas and formation brine would initially migrate out of the source rocks (primary hydrocarbon migration) and into nearby formations as a result of buoyancy and hydrodynamics processes. The geochemistry of these fluids would record an initial C_1/C_2+ , $\delta^{13}\text{C}-\text{CH}_4$, $\delta^2\text{H}-\text{CH}_4$, $\delta^{13}\text{C}-\text{C}_2\text{H}_6$, and noble gas composition, which varies according to thermal conditions of gas generation. As two-phase fluid migration proceeds from the hydrocarbon source to reservoirs and eventually shallow aquifers, solubility partitioning will fractionate the gas components according to their respective solubilities. Solubility partitioning would fractionate the gas components leading to increases in the initial C_1/C_2+ but negligible changes in the $\delta^{13}\text{C}-\text{CH}_4$, $\delta^2\text{H}-\text{CH}_4$, or $\delta^{13}\text{C}-\text{C}_2\text{H}_6$, while also leading to increases in diagnostic noble gas tracers (e.g., $^{20}\text{Ne}/^{36}\text{Ar}$, $^4\text{He}/\text{CH}_4$). Once this postgenetically modified natural gas reached shallow aquifers, it can then mix with variable amounts of biogenic methane. This late stage of mixing with biogenic methane in shallow aquifers would decrease the $\delta^{13}\text{C}-\text{CH}_4$ of methane in shallow aquifers.

Alternative theories may include oxidation or other forms of transport-induced fractionation (e.g., adsorption, diffusion, and dispersion). We suggest that the key to evaluating these processes is understanding the degree of fractionation imparted by various transport phenomena and/or oxidation. Significant volumes of previous work

have demonstrated the diffusion and dispersion are not viable mechanisms for the fractionation of the C_1/C_2+ (reviewed in Darrah et al. 2015b). However, because both solubility partitioning and oxidation remain viable mechanisms, we briefly compare them here.

Because the relative solubility of C_1 and C_2+ vary by approximately $2\times$ (i.e., 200%), while $^{12}C^1H_4$ is only 0.05% to 0.1% (0.5‰ to 1.0‰) less soluble than $^{12}CD^1H_3$ or $^{13}C^1H_4$, one would anticipate the C_1/C_2+ composition of a natural gas could increase dramatically relative to $\delta^{13}C-CH_4$ if solubility partitioning occurred during fluid migration. Similar increases in C_1/C_2+ could result from aerobic oxidation, while anaerobic oxidation would actually decrease the C_1/C_2+ and therefore can be discounted as a mechanism to describe natural gas with this composition (Etiopie et al. 2009; Etiopie and Ciccioli 2009). Therefore, it is reasonable to conclude that mixing with biogenic methane following either solubility partitioning or oxidation could produce a natural gas with both elevated C_1/C_2+ and more negative $\delta^{13}C-CH_4$ (^{12}C enriched) in the resulting mixture.

The challenge is distinguishing fractionation induced by solubility partitioning from that induced by aerobic oxidation. To do this, we must again consider the consortium of data simultaneously. Solubility fractionation would not appreciably change the residual the $\delta^{13}C-CH_4$, δ^2H-CH_4 , or $\delta^{13}C-C_2H_6$, whereas aerobic oxidation would lead to a progressive enrichment in these components (and increase the C_1/C_2+ in the residual natural gas). Conversely, solubility partitioning would increase the ratio of diagnostic noble gas tracers (e.g., $^{20}Ne/^{36}Ar$), while aerobic oxidation would leave this ratio unchanged. Because data from the current study display elevated $\delta^{13}C-CH_4$, $\delta^{13}C-C_2H_6$, and C_1/C_2+ in the inferred migrated thermogenic endmember, it is unclear if we can definitively distinguish between solubility partitioning and oxidation processes. However, because the thermogenic endmember also demonstrates elevated $^{20}Ne/^{36}Ar$ values, we suggest that solubility partitioning must account for at least some of the observed postgenetic modification of the thermogenic endmember, specifically the C_1/C_2+ . It is interesting to note that, like other petroleum basins around the world, if one considers postgenetic modification of a migrated thermogenic gas, the majority of the data can be accounted for by simple two-component mixing between a biogenic endmember and a thermogenic endmember that previously experienced postgenetic modification (Figure 4B).

The Migration and Influence of Fluids from Depth

Previous work from the Karoo Basin suggests that, like other petroleum basins, discrete conduits of hydrocarbon and salt water discharge throughout the Karoo Basin are often located in close proximity to conventional stratigraphic and structural hydrocarbon traps (Rowell and De Swardt 1976; Talma and Esterhuysen 2015). These observations suggest that regional-scale structural geology and the

occurrence of planar discontinuities (i.e., faults and fractures) likely regulate the migration of hydrocarbon gases and salts from depth to the shallow aquifers.

Many aspects of the geochemistry of hydrocarbon gases and saline fluids in the Karoo Basin are also similar to other petroleum basins that have been examined around the world. For example, remnants of more deeply-sourced high-salinity formation waters from the Karoo Basin observed in shallow groundwater as part of this study have been diluted by meteoric water in multiple stages (i.e., both prior to and during the migration of hydrocarbon- and salt-rich fluids to near-surface formations), leading to the paradoxical observation of Modern tritium-active water in the presence of highly saline, thermogenic methane-rich groundwater with extremely long apparent mean residence times (Harkness et al. 2018). It is important to remember that these observations from the Karoo Basin are consistent with a growing number of observations from shallow aquifers in other petroleum basins around the world (Darrah et al. 2014; Moritz et al. 2015; Darrah et al. 2015a, 2015b; Humez et al. 2016; Wen et al. 2016; Harkness et al. 2017b; 2018).

Consistent with Harkness et al. (2018), we observe a striking spatial relationship between samples with highly elevated 4He concentrations, $^4He/CH_4$, $^4He/^{20}Ne$, $^{20}Ne/^{36}Ar$, and zones of intense fracturing related to the intrusion of the dolerite sills. The significant excesses of 4He distinguish the presence of quantifiable fluxes of exogenous fluids to shallow aquifers across the Karoo and suggest that the highly fractured zones near dolerite sills likely provided preferential pathways for the transmission of deeper, saline- and methane-rich fluids to the shallow aquifers on yet unknown geological timescales. In addition to serving as pathways for fluid migration from depth, the zones of intense fracturing near dolerite intrusions also likely remain as preferential pathways for fluid migration within shallow aquifers in this region today. The latter point stems from the fact that shallow aquifers in the region consist of dominantly low porosity and low permeability rocks (Le Maitre et al. 2009; Rosewarne et al. 2013), which is consistent with recent numerical simulations and highlights the importance of fractures in controlling the rate and distribution of gas migration in low permeability formations (Moortgat et al. 2018).

The presence of mantle-derived helium (up to 1%) in groundwater samples rich in methane and salt further supports our interpretation for the presence of exogenous sources of natural gas in the shallow aquifers in the Karoo Basin (Figure 8). Each of the samples with methane concentrations exceeding 14 ccSTP/kg displayed helium isotopic compositions (i.e., $^3He/^4He$ reported as R/R_A) above the anticipated crustal production ratio ($0.02R_A$) commonly observed in thermogenic natural gas (Ballentine et al. 2002; Ballentine and Burnard 2002). Importantly, samples with elevated helium isotopic compositions also displayed He/Ne more than 100 times atmospheric levels precluding atmospheric contamination or tritogenic 3He as a viable source for the elevated levels

of ^3He . Additionally, the presence of elevated $^3\text{He}/^4\text{He}$, specifically within helium-rich samples, provides support for the hypothesis that thermogenic methane- and salt-rich fluids migrated to the near-surface aquifers along preferential pathways induced by the presence of dolerite intrusions.

Mantle-derived fluids (e.g., ^3He and CO_2) can be degassed from an intrusive igneous body, such as the dolerite intrusions commonly observed across the Karoo Basin (Ballentine and Sherwood Lollar 2002; Darrah et al. 2015b; Moore et al. 2018). Following the emplacement of magmatic intrusions, mantle-derived ^3He can be stored within sedimentary reservoirs, such as structural or stratigraphic hydrocarbon traps, for extended periods of geological time and can subsequently mix with or migrate into regions of locally produced fluids (Ballentine and Sherwood Lollar 2002). It remains unclear if these resolvable mantle contributions are related to the dolerite intrusions or serve as evidence for active fluid migration along preferential migration pathways. We do note that it is intriguing that the samples with the highest $^3\text{He}/^4\text{He}$ ratios are those with the highest proportions of methane and salinity, which could suggest that the same deep-reaching conduits that provided preferential pathways for magmatically derived volatiles also permit the migration of thermogenic natural gas and brines to the shallow aquifers in the region.

Conclusion

Global Context for the Occurrence of Biogenic and Thermogenic Natural Gas

Within the Karoo Basin, the subset of methane- and salt-rich samples displays a higher proportion of thermogenic natural gas, whereas the low-salinity freshwaters display almost exclusively low abundances of microbial methane derived via a variety of methanogenic pathways. These trends, recorded in pristine aquifers without any history of conventional or unconventional energy extraction or mining, are broadly consistent with a growing body of data that document a naturally occurring background of elevated levels of *thermogenic* natural gas in aquifers overlying petroleum systems in the USA and Canada (e.g., Warner et al. 2013; Moritz et al. 2015; Darrah et al. 2015b; Humez et al. 2016; Nicot et al. 2017a; Harkness et al. 2017b; Nicot et al. 2017b, 2017c). Furthermore, these data confirm the relationship between a naturally occurring background of *thermogenic* natural gas and elevated levels of salts with a NaCl-type composition. By comparison, the low, natural presence of microbial methane occurs in freshwater and can be clearly distinguished by the molecular and isotopic composition of hydrocarbons and the elemental and isotopic abundances of noble gases. Each of these factors is important to consider in future studies that examine the occurrence of methane in shallow aquifers or stray gas investigations. In addition to evaluating the characteristics of methane occurrence and source, we

document the utility of integrating multiple geochemical tracers (hydrocarbon molecular and isotopic composition, noble gases, and water chemistry) when evaluating the occurrences, sources, and processes that regulate naturally occurring methane contamination in shallow aquifers. The integration of these techniques is specifically important in light of the growing realization that the geochemical composition of naturally occurring methane has experienced alteration by postgenetic modification in the subsurface.

Acknowledgments

We acknowledge financial support from NSF EAGER (EAR-1249255), NSF SusChem (EAR-1441497), and DOE (DE-FE0024357) to T.H.D. We would also like to thank the members of the School of Earth Sciences (OSU) and the Nicholas School of the Environment (Duke) for assisting in data analysis and constructive feedback on this project. Additionally, this work would not be possible without the cooperation with farmers and property owners across the Karoo Basin and their hospitality during sample collection. Finally, we'd like to express gratitude to Ryno Botha and Andrew Watson who were essential for completing the field work.

Authors' Note:

The authors do not have any conflicts of interest or financial disclosures to report.

References

- Aarnes, I., H. Svensen, S. Polteau, and S. Planke. 2011. Contact metamorphic devolatilization of shales in the Karoo Basin, South Africa, and the effects of multiple sill intrusions. *Chemical Geology* 281, no. 3: 181–194.
- Adams, S., R. Titus, K. Pieterse, G. Tredoux, and C. Harris. 2001. Hydrochemical characteristics of aquifers near Sutherland in the Western Karoo, South Africa. *Journal of Hydrology* 241: 91–103.
- Baldassare, F.J., M.A. McCaffrey, and J.A. Harper. 2014. A geochemical context for stray gas investigations in the northern Appalachian Basin: Implications of analyses of natural gases from Neogene-through Devonian-age strata. *AAPG Bulletin* 98, no. 2: 341–372.
- Ballentine, C.J., and P.G. Burnard. 2002. Production, release and transport of noble gases in the continental crust. In *Noble Gases in Geochemistry and Cosmochemistry. Reviews in Mineralogy & Geochemistry*, ed. D. Porcelli, C.J. Ballentine, and R. Wieler, 481–538. Chantilly, Virginia: Mineralogical Society of America.
- Ballentine, C.J., and B. Sherwood Lollar. 2002. Regional groundwater focusing of nitrogen and noble gases into the Hugoton-panhandle giant gas field, USA. *Geochimica et Cosmochimica Acta* 66, no. 14: 2483–2497.
- Ballentine, C.J., R. Burgess, and B. Marty. 2002. Tracing fluid origin, transport and interaction in the crust. In *Noble Gases in Geochemistry and Cosmochemistry. Reviews in Mineralogy & Geochemistry*, ed. D. Porcelli, C.J. Ballentine, and R. Wieler, 539–614. Chantilly, Virginia: Mineralogical Society of America.
- Barry, P.H., M. Lawson, W.P. Meurer, O. Warr, J.C. Mabry, D.J. Byrne, and C.J. Ballentine. 2016. Noble gases solubility

- models of hydrocarbon charge mechanism in the Sleipner Vest gas field. *Geochimica et Cosmochimica Acta* 194: 291–309.
- Bernard, B.B., J.M. Brooks, and W.M. Sackett. 1976. Natural-gas seepage in Gulf of Mexico. *Earth and Planetary Science Letters* 31, no. 1: 48–54.
- Brantley, S.L., D. Yoxtheimer, S. Arjmand, P. Grieve, R. Vidic, J. Pollak, G.T. Llewellyn, J. Abad, and C. Simon. 2014. Water resource impacts during unconventional shale gas development: The Pennsylvania experience. *International Journal of Coal Geology* 126: 140–156.
- Catuneanu, O., H. Wopfner, P.G. Eriksson, B. Cairncross, B.S. Rubidge, R.M.H. Smith, and P.J. Hancox. 2005. The Karoo Basins of south-central Africa. *Journal of African Earth Sciences* 43: 211–253.
- Darrah, T.H. 2018. Time to settle the fracking controversy. *Groundwater* 56, no. 2: 1–2.
- Darrah, T.H., and R.J. Poreda. 2012. Evaluating the accretion of meteoritic debris and interplanetary dust particles in the GPC-3 sediment core using noble gas and mineralogical tracers. *Geochimica et Cosmochimica Acta* 84: 329–352.
- Darrah, T.H., D. Tedesco, F. Tassi, O. Vaselli, E. Cuoco, and R.J. Poreda. 2013. Gas chemistry of the Dallol region of the Danakil depression in the afar region of the northern-most east African rift. *Chemical Geology* 339: 16–29.
- Darrah, T.H., R.B. Jackson, A. Vengosh, N.R. Warner, and R.J. Poreda. 2014. *Noble Gases Identify the Presence and Mechanisms of Stray Gas Contamination in the Marcellus and Barnett Shales*. Washington, DC: US National Academy of Science.
- Darrah, T.H., R.B. Jackson, A. Vengosh, N.R. Warner, and R.J. Poreda. 2015a. Noble gases: A new technique for fugitive gas investigation in groundwater. *Groundwater* 53, no. 1: 23–28.
- Darrah, T.H., R.B. Jackson, A. Vengosh, N.R. Warner, C.J. Whyte, T.B. Walsh, A.J. Kondash, and R.J. Poreda. 2015b. The evolution of Devonian hydrocarbon gases in shallow aquifers of the northern Appalachian Basin: Insights from integrating noble gas and hydrocarbon geochemistry. *Geochimica et Cosmochimica Acta* 170: 321–355.
- Etioppe, G., and P. Ciccioli. 2009. Earth's degassing: A missing ethane and propane source. *Science* 323, no. 5913: 478–478.
- Etioppe, G., A. Feyzullayev, and C.L. Baci. 2009. Terrestrial methane seeps and mud volcanoes: A global perspective of gas origin. *Marine and Petroleum Geology* 26, no. 3: 333–344.
- Harkness, J.S., T.H. Darrah, M.T. Moore, C.J. Whyte, P.D. Mathewson, T. Cook, and A. Vengosh. 2017a. Naturally occurring versus anthropogenic sources of elevated molybdenum in groundwater: Evidence for Geogenic contamination from Southeast Wisconsin, United States. *Environmental Science & Technology* 51, no. 21: 12190–12199.
- Harkness, J.S., T.H. Darrah, N.R. Warner, C.J. Whyte, M.T. Moore, R. Millot, W. Kloppmann, R.B. Jackson, and A. Vengosh. 2017b. The geochemistry of naturally occurring methane and saline groundwater in an area of unconventional shale gas development. *Geochimica et Cosmochimica Acta* 208: 302–334.
- Harkness, J.S., et al. 2018. Baseline groundwater GeoChemistry in the Karoo Basin, South Africa. *Groundwater* 56, no. 2: 1–18.
- Heilweil, V.M., P.L. Grieve, S.A. Hynek, S.L. Brantley, D.K. Solomon, and D.W. Risser. 2015. Stream measurements locate thermogenic methane fluxes in groundwater discharge in an area of shale-gas development. *Environmental Science & Technology* 49, no. 7: 4057–4065.
- Humez, P., B. Mayer, J. Ing, M. Nightingale, V. Becker, A. Kingston, O. Akbilgic, and S. Taylor. 2016. Occurrence and origin of methane in groundwater in Alberta (Canada): Gas geochemical and isotopic approaches. *Science of the Total Environment* 541: 1253–1268.
- Hunt, A.G., T.H. Darrah, and R.J. Poreda. 2012. Determining the source and genetic fingerprint of natural gases using noble gas geochemistry: A northern Appalachian Basin case study. *AAPG Bulletin* 96, no. 10: 1785–1811.
- Jackson, R.B., A. Vengosh, T.H. Darrah, N.R. Warner, A. Down, R.J. Poreda, S.G. Osborn, K. Zhao, and J.D. Karr. 2013. Increased stray gas abundance in a subset of drinking water wells near Marcellus shale gas extraction. *Proceedings of the National Academy of Sciences of the United States of America* 110, no. 28: 11250–11255.
- Johnson, M.R., C.J. Van Vuuren, W.F. Hegenberger, R. Key, and U. Shoko. 1996. Stratigraphy of the Karoo Supergroup in southern Africa: An overview. *Journal of African Earth Sciences* 23, no. 1: 3–15.
- Johnson, M.R., et al. 2006. Sedimentary rocks of the Karoo Supergroup. In *Geological Society of South Africa and Council for Geoscience, Johannesburg and Pretoria, South Africa*, ed. M.R. Johnson, C.R. Anhaeusser, and R.J. Thomas, 461–499. Johannesburg, South Africa: Geological Society of South Africa.
- Kang, M., S. Christian, M.A. Celia, D.L. Mauzerall, M. Bill, A.R. Miller, Y. Chen, M.E. Conrad, T.H. Darrah, and R.B. Jackson. 2016. Identification and characterization of high methane-emitting abandoned oil and gas wells. *Proceedings of the National Academy of Sciences of the United States of America* 113, no. 48: 13636–13641.
- Le Maltre, D., C. Colvina, and A. Maherrya. 2009. Water resources in the Klein Karoo: The challenge of sustainable development in a water-scarce area. *South African Journal of Science* 105: 39–48.
- Mahed, G. 2016. Development of a conceptual geohydrological model for a fractured rock aquifer in the Karoo, near Sutherland, South Africa. *South African Journal of Geology* 119, no. 1: 33–38.
- McMahon, P.B., R.R. Caldwell, J.M. Galloway, J.F. Valder, and A.G. Hunt. 2015. Quality and age of shallow groundwater in the Bakken formation production area, Williston Basin, Montana and North Dakota. *Groundwater* 53: 81–94.
- Molofsky, L.J., J.A. Connor, A.S. Wylie, T. Wagner, and S.K. Farhat. 2013. Evaluation of methane sources in groundwater in northeastern Pennsylvania. *Ground Water* 51, no. 3: 333–349.
- Moore, M.T., D.S. Vinson, C.J. Whyte, W.K. Eymold, T.B. Walsh, and T.H. Darrah. 2018. Differentiating between biogenic and thermogenic sources of natural gas in coalbed methane reservoirs from the Illinois Basin using noble gas and hydrocarbon geochemistry. In *From Source to Seep: Geochemical Applications in Hydrocarbon Systems*, ed. M. Lawson, M. J. Formolo, and J. M. Eiler. London, UK: Geological Society of London, Special Publication no. 468. <https://doi.org/10.1144/SP468.8>
- Moortgat, J.B., F.W. Schwartz, and T.H. Darrah. 2018. Numerical modeling of methane leakage from a faulty natural-gas-well into fractured tight formations. *Groundwater* 56, no. 2: 1–12.
- Moritz, A., J.F. Hélie, D.L. Pinti, M. Larocque, D. Barnetche, S. Retailleau, R. Lefebvre, and Y. Gélinas. 2015. Methane baseline concentrations and sources in shallow aquifers from the shale gas-prone region of the St. Lawrence lowlands (Quebec, Canada). *Environmental Science & Technology* 49, no. 7: 4765–4771.
- Murray, R. 2015. The Use of Chemistry, Isotopes and Gases as Indicators of Deeper Circulating Groundwater in the Main Karoo Basin, Water Research Commission, Report to the Water Research Commission.
- Nicot, J.P., T. Larson, R. Darvari, P. Mickler, M. Sloten, J. Aldridge, K. Uhlman, and R. Costley. 2017a. Controls on methane occurrences in shallow aquifers overlying the

- Haynesville shale gas field, East Texas. *Groundwater* 55, no. 4: 443–454.
- Nicot, J.P., T. Larson, R. Darvari, P. Mickler, K. Uhlman, and R. Costley. 2017b. Controls on methane occurrences in aquifers overlying the eagle ford shale play, South Texas. *Groundwater* 55, no. 4: 455–468.
- Nicot, J.P., P. Mickler, T. Larson, M. Clara Castro, R. Darvari, K. Uhlman, and R. Costley. 2017c. Methane occurrences in aquifers overlying the Barnett shale play with a focus on Parker County, Texas. *Groundwater* 55, no. 4: 469–481.
- Oesterlen, P.M. 1991. A further report on the geology of the Dande west area (western Cabora Bassa Basin, mid-Zambezi Valley). *Annales Zimbabwean Geological Society* 15: 1–5.
- Osborn, S.G., A. Vengosh, N.R. Warner, and R.B. Jackson. 2011. Methane contamination of drinking water accompanying gas-well drilling and hydraulic fracturing. *Proceedings of the National Academy of Sciences of the United States of America* 108, no. 20: 8172–8176.
- Prinzhofer, A., and E. Pernaton. 1997. Isotopically light methane in natural gas: Bacterial imprint or diffusive fractionation? *Chemical Geology* 142, no. 3–4: 193–200.
- Revesz, K.M., K.J. Breen, A.J. Baldassare, and R.C. Burruss. 2012. Carbon and hydrogen isotopic evidence for the origin of combustible gases in water-supply wells in north-central Pennsylvania (vol 25, pg 1845, 2010). *Applied Geochemistry* 27, no. 1: 360–375.
- Rosewarne, P.N. et al. 2013. *Karoo Groundwater Atlas*. Johannesburg, South Africa: Geological Society of South Africa.
- Roswell, D.M., and A.M.J. De Swardt. 1976. Diagenesis in cape and Karroo sediments, South Africa, and its bearing on their hydrocarbon potential. *Transactions of the Geological Society of South Africa* 79, no. 1: 81–145.
- Schoell, M. 1983. Genetic characterization of natural gases. *AAPG Bulletin-American Association of Petroleum Geologists* 67, no. 12: 2225–2238.
- Sherwood, O.A., J.D. Rogers, G. Lackey, T.L. Burke, S.G. Osborn, and J.N. Ryan. 2016. Groundwater methane in relation to oil and gas development and shallow coal seams in the Denver-Julesburg Basin of Colorado. *Proceedings of the National Academy of Sciences of the United States of America* 113, no. 30: 8391–8396.
- Siegel, D.I., N.A. Azzolina, B.J. Smith, A.E. Perry, and R.L. Bothun. 2015. Methane concentrations in water wells unrelated to proximity to existing oil and gas wells in northeastern Pennsylvania. *Environmental Science & Technology* 49, no. 7: 4106–4112.
- Swana, K. 2016. *Application of Hydrochemistry and Residence Time Constraints to Distinguish Groundwater Systems in the Karoo Basin Prior to Shale-Gas Exploration*. Matieland, South Africa: Stellenbosch University.
- Talma, S., and C. Esterhuysen. 2015. Natural methane in the Karoo: Its occurrence and isotope clues to its origin. *South African Journal of Geology* 118: 45–54.
- USGS. 2011. *National Field Manual for the Collection of Water-Quality Data*. Washington, DC: US Geological Survey.
- Vengosh, A., R.B. Jackson, N. Warner, T.H. Darrah, and A. Kondash. 2014. A critical review of the risks to water resources from unconventional shale gas development and hydraulic fracturing in the United States. *Environmental Science & Technology* 48, no. 15: 8334–8348.
- Vinson, D.S., N.E. Blair, A.M. Martini, S. Larter, W.H. Orem, and J.C. McIntosh. 2017. Microbial methane from in situ biodegradation of coal and shale: A review and reevaluation of hydrogen and carbon isotope signatures. *Chemical Geology* 453: 128–145.
- Warner, N.R., R.B. Jackson, T.H. Darrah, S.G. Osborn, A. Down, K. Zhao, A. White, and A. Vengosh. 2012a. Geochemical evidence for possible natural migration of Marcellus formation brine to shallow aquifers in Pennsylvania. *Proceedings of the National Academy of Sciences of the United States of America* 109, no. 30: 11961–11966.
- Warner, N.R., R.B. Jackson, T.H. Darrah, S.G. Osborn, A. Down, K. Zhao, A. White, and A. Vengosh. 2012b. Reply to Engelder: Potential for fluid migration from the Marcellus formation remains possible. *Proceedings of the National Academy of Sciences of the United States of America* 109, no. 52: E3626.
- Warner, N.R., T.M. Kresse, P.D. Hays, A. Down, J.D. Karr, R.B. Jackson, and A. Vengosh. 2013. Geochemical and isotopic variations in shallow groundwater in areas of the Fayetteville shale development, north-central Arkansas. *Applied Geochemistry* 35: 207–220.
- Warner, N.R., T.H. Darrah, R.B. Jackson, R. Millot, W. Kloppmann, and A. Vengosh. 2014. New tracers identify hydraulic fracturing fluids and accidental releases from oil and gas operations. *Environmental Science & Technology* 48, no. 21: 12552–12560.
- Wen, T., M.C. Castro, J.P. Nicot, C.M. Hall, T. Larson, P. Mickler, and R. Darvari. 2016. Methane sources and migration mechanisms in shallow groundwaters in Parker and Hood counties, Texas- a heavy noble gas analysis. *Environmental Science & Technology*.
- Whiticar, M.J. 1999. Carbon and hydrogen isotope systematics of bacterial formation and oxidation of methane. *Chemical Geology* 161, no. 1–3: 291–314.
- Whiticar, M.J., E. Faber, and M. Schoell. 1986. Biogenic methane formation in marine and fresh-water environments- CO₂ reduction vs. acetate fermentation isotope evidence. *Geochimica et Cosmochimica Acta* 50, no. 5: 693–709.
- Whiticar, M.J., E. Faber, J.K. Whelan, and B.R.T. Simoneit. 1994. Thermogenic and bacterial hydrocarbon gases (Free and sorbed) in Middle Valley, Juan De Fuca Ridge, LEG 139. Proceedings of the Ocean Drilling Program, Scientific Results, 139: 467–477.
- Woodford, A.C., and L. Chevallier. 2002. *Hydrogeology of the Karoo Basin: Current Knowledge and Future Needs, Pretoria*. Pretoria, South Africa: Water Research Commission.